

Unraveling the Heater: New Insights into the Structure of the Alternative Oxidase

Anthony L. Moore,¹ Tomoo Shiba,² Luke Young,¹ Shigeharu Harada,³ Kiyoshi Kita,² and Kikukatsu Ito⁴

¹Biochemistry and Molecular Biology, School of Life Sciences, University of Sussex, Brighton BN1 9QG, United Kingdom; email: a.l.moore@sussex.ac.uk

²Department of Biomedical Chemistry, Graduate School of Medicine, University of Tokyo, Tokyo 113-0033, Japan

³Department of Applied Biology, Graduate School of Science and Technology, Kyoto Institute of Technology, Kyoto 606-8585, Japan

⁴Cryobiofrontier Research Center, Faculty of Agriculture, Iwate University, Morioka 020-8550, Japan

Annu. Rev. Plant Biol. 2013. 64:637–63

The *Annual Review of Plant Biology* is online at plant.annualreviews.org

This article's doi:

10.1146/annurev-arplant-042811-105432

Copyright © 2013 by Annual Reviews.

All rights reserved

Keywords

electron transport, cytochrome pathway, diiron carboxylate proteins, respiration, ubiquinol oxidase, NADH dehydrogenases

Abstract

The alternative oxidase is a membrane-bound ubiquinol oxidase found in the majority of plants as well as many fungi and protists, including pathogenic organisms such as *Trypanosoma brucei*. It catalyzes a cyanide- and antimycin-A-resistant oxidation of ubiquinol and the reduction of oxygen to water, short-circuiting the mitochondrial electron-transport chain prior to proton translocation by complexes III and IV, thereby dramatically reducing ATP formation. In plants, it plays a key role in cellular metabolism, thermogenesis, and energy homeostasis and is generally considered to be a major stress-induced protein. We describe recent advances in our understanding of this protein's structure following the recent successful crystallization of the alternative oxidase from *T. brucei*. We focus on the nature of the active site and ubiquinol-binding channels and propose a mechanism for the reduction of oxygen to water based on these structural insights. We also consider the regulation of activity at the posttranslational and retrograde levels and highlight challenges for future research.

Contents

INTRODUCTION	638
HISTORICAL PERSPECTIVES	638
GENERAL CHARACTERISTICS OF CYANIDE-INSENSITIVE RESPIRATION	639
OVERALL THREE-DIMENSIONAL STRUCTURE OF AOX	642
Resolution of the Active Site	645
Role of Tyrosines	646
Ubiquinol-Binding Sites	646
Roles and Locations of Universally Conserved Residues	651
Catalytic Mechanism for the Reduction of Oxygen to Water ..	652
NATIVE STRUCTURE OF AOX IN THERMOGENIC PLANTS	654
POSTTRANSLATIONAL REGULATION OF AOX ACTIVITY IN THERMOGENIC PLANTS	654
N-TERMINAL EXTENSION AND STRUCTURAL-FUNCTIONAL CONSIDERATIONS	655
RETROGRADE REGULATION OF AOX	655

INTRODUCTION

The alternative oxidase (AOX) is a terminal ubiquinol oxidase that in eukaryotes is located on the substrate side of the cytochrome *bc*₁ complex in the mitochondrial respiratory chain. It is virtually ubiquitous within the plant kingdom and is also found in many fungi and protists, including pathogenic organisms such as *Trypanosoma brucei* and *Cryptosporidium parvum*. Homologs have also been identified in α -proteobacteria and are emerging in a broad range of animal species, and its distant relative, the plastid terminal oxidase, has been identified in cyanobacteria (75). The functions of AOXs are highly diverse and typically include thermogenesis, stress tolerance (particularly to stresses

induced by the generation of reactive oxygen species), and the maintenance of mitochondrial and cellular homeostasis, to name but a few (40).

AOX has been widely researched, yet until recently we knew very little about its three-dimensional structure. Knowledge of the structure-function relationships of AOX is fundamental to a fuller understanding of how the protein operates in planta and, in particular, its role in regulating plant growth and development. The ability of the plant cell to maintain energy homeostasis, particularly under biotic and abiotic stresses, is central to plant survival under such conditions. To understand the roles that AOX plays in defending against such metabolic fluctuations, we need to determine how its structure enables it to perform such functions.

A long-term pursuit in AOX research has been the identification of suitable expression and purification conditions to facilitate the crystallization of the protein. In this review, we restrict our discussion to the recent structural insights into AOXs following the crystallization of the trypanosomal alternative oxidase (TAO) along with how changes in structure might influence function. For fuller descriptions of the function and regulation of AOX both in vitro and in vivo, readers are referred to other reviews and publications (4, 40, 61, 77, 78, 98, 117, 124, 125).

HISTORICAL PERSPECTIVES

The observation that plants can raise their temperature above the ambient temperature (i.e., are thermogenic) was first published in 1778 by Lamarck (73), who noted that the spadices of certain plants (Araceae) were “hot to the point of boiling” (pp. 537–38). Approximately 100 years later, in an 1877 letter to his friend the Marchese Corsi-Salviati, the illustrious explorer and botanist Dr. Eduardo Beccari reported his discovery of a gigantic aroid (*Amorphophallus titanum*) in Sumatra (12, 55). These findings were confirmed in 1885 by Henry Forbes (see 55), who stumbled across this magnificent plant during his wanderings in

AOX: alternative oxidase

TAO: trypanosomal alternative oxidase

the eastern archipelago. Beccari subsequently sent tubers and seeds of this plant to the Marchese in Florence. Unfortunately, the tubers did not arrive owing to import restrictions in Marseilles, but the seeds did, and under careful supervision they germinated in the Marchese's garden. On Beccari's request, young plants were transported to Kew Gardens, and the first *Amorphophallus* flowering outside of its native Sumatra occurred in June 1889.

Aroids were not the only plants to be observed to have thermogenic properties. For instance, in 1851 Garreau (47) noted a close relationship between respiration and heat development, and in 1855 Caspary (26) demonstrated that the flower temperature of *Victoria regia* rose 15°C above ambient during flowering and noted that "the chemical process that is happening at that moment is a very vivid process which has been called 'burning' and that the source of heat is due to oxygen intake" (p. 753)—a remarkable conclusion given the simplicity of the measurements. In 1898 Miyake (83) observed that the flowering of *Nelumbo nucifera* was also associated with a temperature rise of 10°C above ambient. Even today, botanical gardens around the world continue to cultivate thermogenic plants because of the great publicity and crowds they draw.

Even given the tremendous insights of Garreau (47), Caspary (26), and Miyake (83), however, the cause of the heat generation by thermogenic plants remained a mystery until 150 years after Lamarck's discovery, when Van Herk (126–128) discovered that respiration in Araceae spadices was remarkably insensitive to inhibition by cyanide and suggested that this could be due to the activity of a respiratory pathway containing a noncytochrome auto-oxidizable flavoprotein. The suggestion that cyanide-insensitive respiration is due to a second respiratory pathway that branches from the main respiratory chain on the substrate side of cytochrome *c* arose from Okunuki's (93) investigations during his study of pollen respiration. James & Beever (62) extended Van Herk's observations to *Arum maculatum*, and James &

Elliott (63) demonstrated that cyanide-insensitive respiration is indeed mitochondrial in origin.

The presence of an auto-oxidizable flavoprotein remained one of the best explanations for the mechanism of heat generation by cyanide-resistant respiration until Bendall & Bonner (15) reviewed the area and the various proposed hypotheses and concluded, in light of new results, that although a flavoprotein was in many ways the most plausible solution, it could not account for the observation that simple flavoprotein oxidases reduce oxygen to hydrogen peroxide rather than water. They further concluded that because the cyanide-resistant respiration could be inhibited by metal chelators, either a nonheme iron or another type of metalloprotein must be the key component of the oxidase. They also raised the question of whether the two pathways competed directly with each other or were regulated in vivo by some controlling switch. The field has certainly advanced significantly in the 40 years since these proposals, but it is interesting to note how close Bendall & Bonner's (15) suggestions match the most recent information on the protein's crystal structure (112).

GENERAL CHARACTERISTICS OF CYANIDE-INSENSITIVE RESPIRATION

Following from Okunuki's (93) work showing that the second oxidase branches from the main respiratory pathway on the substrate side of cytochrome *c*, numerous investigations have confirmed not only that this is the case, but also that the pathway branches at the level of the ubiquinone pool (105), consistent with the oxidase being non-protonmotive (87). **Figure 1** shows a generally accepted scheme of the respiratory chain, including the location of AOX along with the currently accepted crystal structures of the four major respiratory chain complexes (complexes I–IV) and the ATP synthase (complex V). (For a detailed description of the composition of these complexes in addition to the numerous internal

Non-protonmotive complex: a respiratory chain complex that does not translocate protons

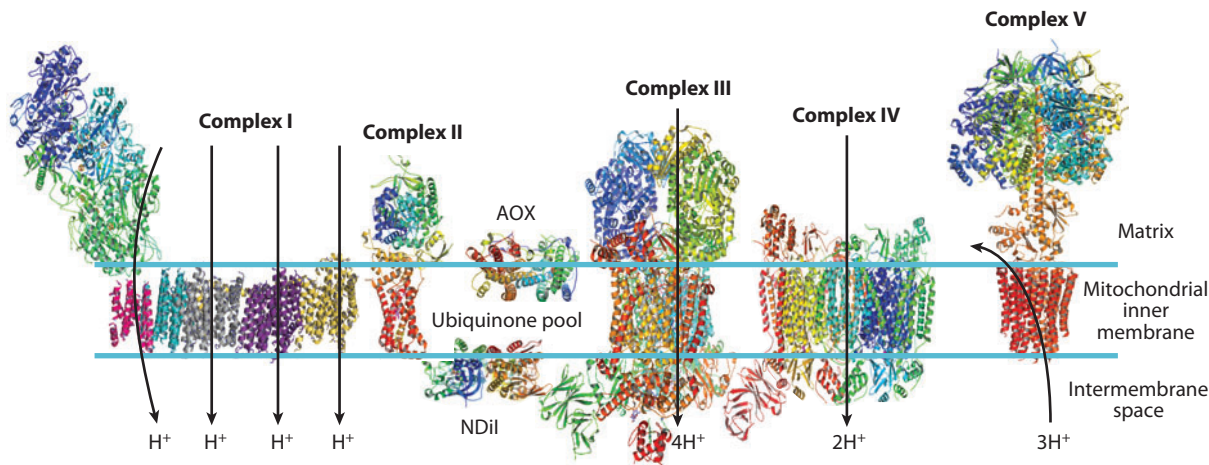


Figure 1

The mitochondrial respiratory chain. The major mitochondrial respiratory complexes are shown as crystal structures where known: complex I, NADH dehydrogenase [Protein Data Bank (PDB) 3M9S (33)]; complex II, succinate dehydrogenase [PDB 3VR8 (113)]; complex III, cytochrome *bc*₁ [PDB 3HIJ 72 (60)]; complex IV, cytochrome *c* oxidase [PDB 10CO (139)]; trypanosomal alternative oxidase [PDB 3VV9 (112)]; yeast NADH dehydrogenase [PDB 4G9K (59)]; and complex V, ATP synthase [F₀, PDB 1C17 (99); F₁, PDB 1E79 (48)]. The stator has not been included, but structures can be found at PDB 2A7U (134) and PDB 1L2P (30).

and external NADH dehydrogenases within the plant respiratory chain, see Reference 79.)

The elegant spectrophotometric studies of Bendall & Bonner (15) clearly demonstrated that the AOX pathway does not contain any chromophores or flavoproteins, and later electron paramagnetic resonance (EPR) studies confirmed that no unique iron-sulfur protein is associated with the oxidase. However, the pathway's ability to reduce oxygen to water requires a transition metal (such as iron), and this idea was supported by the finding that metal chelators (such as primary hydroxamic acids) potently inhibit cyanide-insensitive respiration (109). Minagawa et al. (81) provided the first compelling evidence that iron is required for AOX synthesis, and this was later confirmed by Ajayi et al. (6) using recombinant TAO expressed in *Escherichia coli*.

Although there have been numerous attempts to purify AOX from a variety of sources (15, 18, 23, 34, 35, 57, 66, 91, 103, 140), none could provide definitive experimental evidence about the nature of the transition metal until the advent of recombinant DNA technology. Following Rhoads & McIntosh's (100) isola-

tion of the first cDNA encoding the AOX gene, Berthold et al. (20) overexpressed the *Ara-bidopsis* *rAOX* gene in *E. coli*, and EPR analysis revealed the presence of a hydroxo-bridged diiron protein at the heart of the oxidase. Later, Moore et al. (88) also found such a signal in isolated mitochondria, purified protein, and recombinant protein. However, Kido et al. (67), using purified TAO protein, were the first to directly demonstrate that AOX contains iron.

The proposal that AOX contains a binuclear nonheme diiron protein initially arose from the modeling studies of Siedow and colleagues (89, 115). Siedow et al. (115) modeled the AOX active site on those found in the diiron group of proteins, such as methane monooxygenase (MMO) and the R2 subunit of ribonucleotide reductase (RNR). The active sites of these proteins contain a four-helix bundle—a common structural element for this group—that acts as a scaffold to bind the binuclear diiron center. In general, the two iron atoms are ligated by four highly conserved glutamate/aspartate residues and two histidine residues, the arrangement of which yields a characteristic signature motif.

MMO: methane monooxygenase

RNR: R2 subunit of ribonucleotide reductase

Although the Siedow et al. (115) model correctly identified AOX as a diiron carboxylate protein, Andersson & Nordlund (11) reassessed this model in view of the finding that the predicted order and length of the helices in the four-helix bundle were substantially different from those of other diiron carboxylate proteins. The Andersson & Nordlund model (11), later refined by Berthold et al. (17), was based on Δ^9 -desaturase and thereby resulted in an arrangement of the metal ligands that was closer to that observed in the R2-type diiron proteins than to that predicted by Siedow et al. (115). More important from a structural perspective, however, was that the revised model contained the evolutionarily conserved protein fold observed in all other diiron proteins and additionally included a hydrophobic crevice leading from the membrane-binding region toward the diiron center, presumably acting as the substrate-binding site (17).

The general consensus from such homology modeling is that AOX is an integral (~32-kDA) interfacial membrane protein that contains a nonheme diiron carboxylate active site and interacts with a single leaflet of the lipid bilayer by two short hydrophobic helices (19) in a manner comparable to prostaglandin H1 synthase (96), squalene cyclase (132), and CLK-1 (14). This model is supported by spectroscopy and extensive site-directed mutagenesis studies (6, 7, 20, 44, 90). Recent reference to the Protein Data Bank data sets (<http://pfam.sanger.ac.uk>) reveals that AOXs are currently the largest group within this family of proteins, being present in at least 270 species and having 580 lodged sequences to date.

Plant AOX has also been predicted to be homodimeric, as is the case for prostaglandin synthase, squalene cyclase, and probably CLK-1 (see 14, 19, 96, 132). Interestingly, homodimers have been proposed to be not universal within the AOX group, as fungal and other nonplant AOXs lack the highly conserved cysteines found in plant AOXs (123). Dimerization does result in constraints on subunit orientation, however, because each hydrophobic domain of each monomer must be within the confines of

the membrane (17), and in the case of the plant enzyme, at least, if the redox-active cysteines do play a role in dimerization, then they must be oriented such that the cysteines of each monomer can interact with one another.

As indicated above, one of the ultimate goals in studying the structure of AOX has been determining a protein crystal structure at sufficient resolution to detect the active site and membrane-binding regions. Although attempts to purify the oxidase from a variety of tissues resulted in purified protein, in general, the lack of yield and relative instability at room temperature have hampered attempts to crystallize the protein (5, 15, 18, 23, 34, 35, 57, 66, 91, 103, 140). A word of caution should be noted, however, with respect to crystallographic structures: Although they are important for an understanding of what the protein looks like, they do provide only a snapshot of the protein in that particular condition and do not necessarily provide full or correct structural details.

Functional expression of TAO (45, 91) and *Arabidopsis thaliana* AOX (AtAOX) (20) at high levels in heme-deficient *E. coli* membranes led to purification protocols that resulted in highly active proteins with remarkable stability. The use of an *E. coli* $\Delta hemA$ mutant strain that lacks cytochromes *bo* and *bd* arose from the earlier studies of Kumar & Soll (72), who discovered that AtAOX expression in this strain rescues aerobic respiration. More recently, Kido et al. (67) refined earlier attempts (45, 91) to over-express recombinant TAO and developed purification protocols that resulted in a purified protein of sufficient yield and purity to enable the first report of an AOX crystal (68).

Purified protein has been used not only for crystallization but also in kinetic and spectroscopic studies. Kinetic results have provided some interesting molecular insights into how AOX, a simple ubiquinol oxidase, can compete effectively with other oxidases. For instance, although the calculated specificity constant (K_{cat}/K_m) for TAO is comparable to that of other oxidases, such as cytochrome *bo* (107), it is outcompeted by the cytochrome *bc*₁ complex (37). As Kido et al. (67) rightly point out,

CLK-1: a small mitochondrial diiron carboxylate enzyme involved in the penultimate step of ubiquinone synthesis

caution should be exercised in interpreting such results because they are performed under non-physiological conditions and substrate concentrations; nevertheless, these results do reveal that AOX is both kinetically and thermodynamically competent to compete with other oxidases in the respiratory chain. The purity and stability of the recombinant protein have also enabled Fourier transform infrared spectroscopy (FTIR) studies (74), which not only confirmed that AOX is indeed a diiron carboxylate protein (in that it revealed clear signals that could be attributed to carboxylate and histidine residues that change during a redox cycle) but also revealed a sharp band that was tentatively attributed to the loss of a tyrosyl radical (74).

OVERALL THREE-DIMENSIONAL STRUCTURE OF AOX

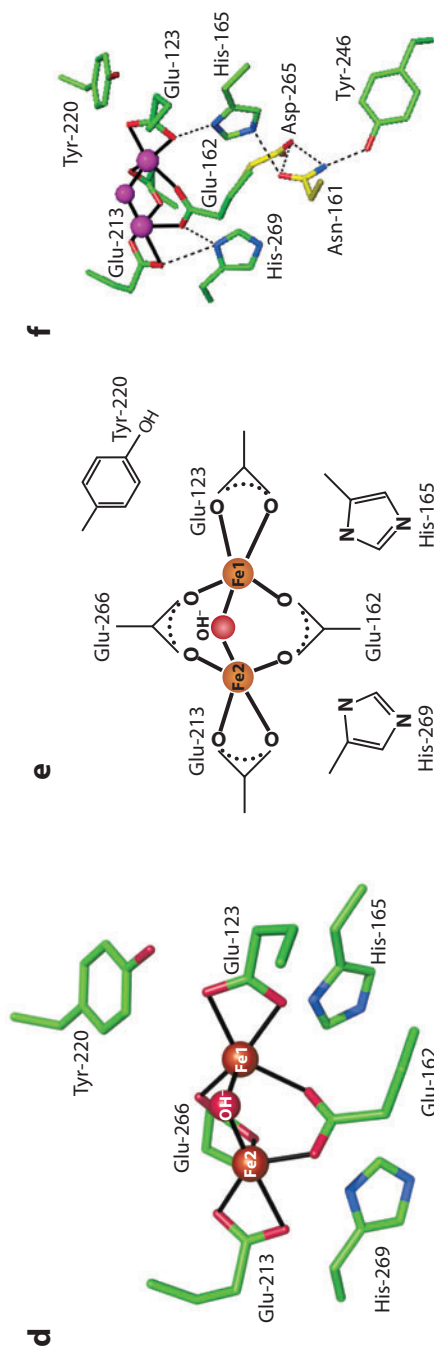
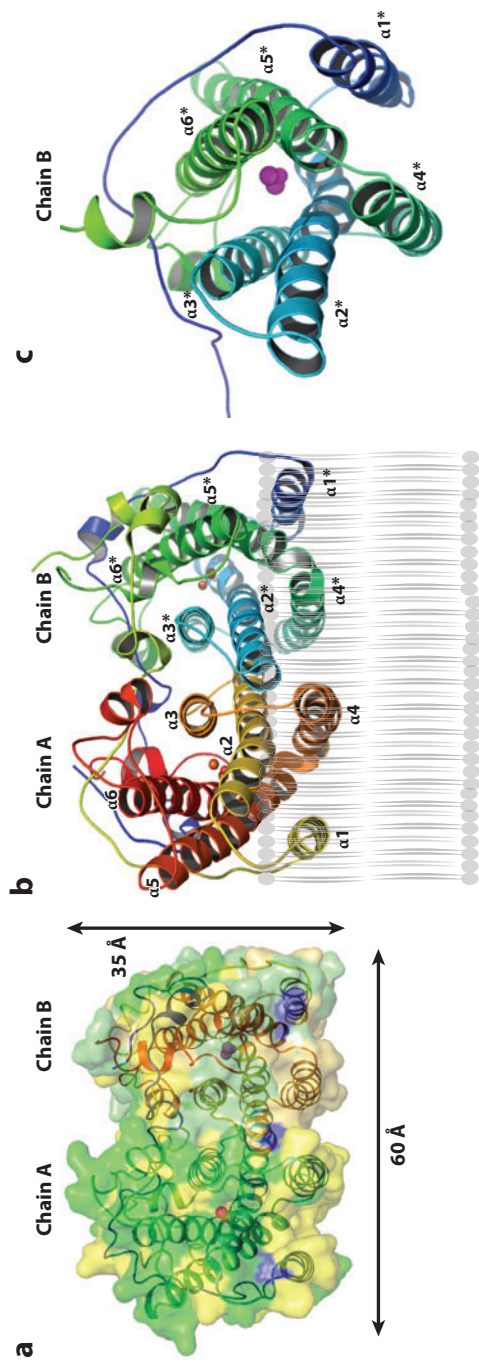
Molecular modeling using MMO, RNR, or Δ^9 -desaturase predicted the presence of a four-helix bundle at the AOX core (19), a characteristic feature of diiron proteins. The TAO crystal structure (112) determined at 2.85-Å resolution indeed confirms that AOX is a diiron carboxylate protein and is dimeric (**Figure 2a**). Each monomer comprises six long helices ($\alpha 1$ to $\alpha 6$) and four short helices ($\alpha S1$ to $\alpha S4$) arranged in an antiparallel fashion, with helices $\alpha 2$, $\alpha 3$, $\alpha 5$, and $\alpha 6$ forming a four-helix bundle (**Figure 2b,c**). Within the dimer (**Figure 2a**), the two monomers are related by a twofold axis

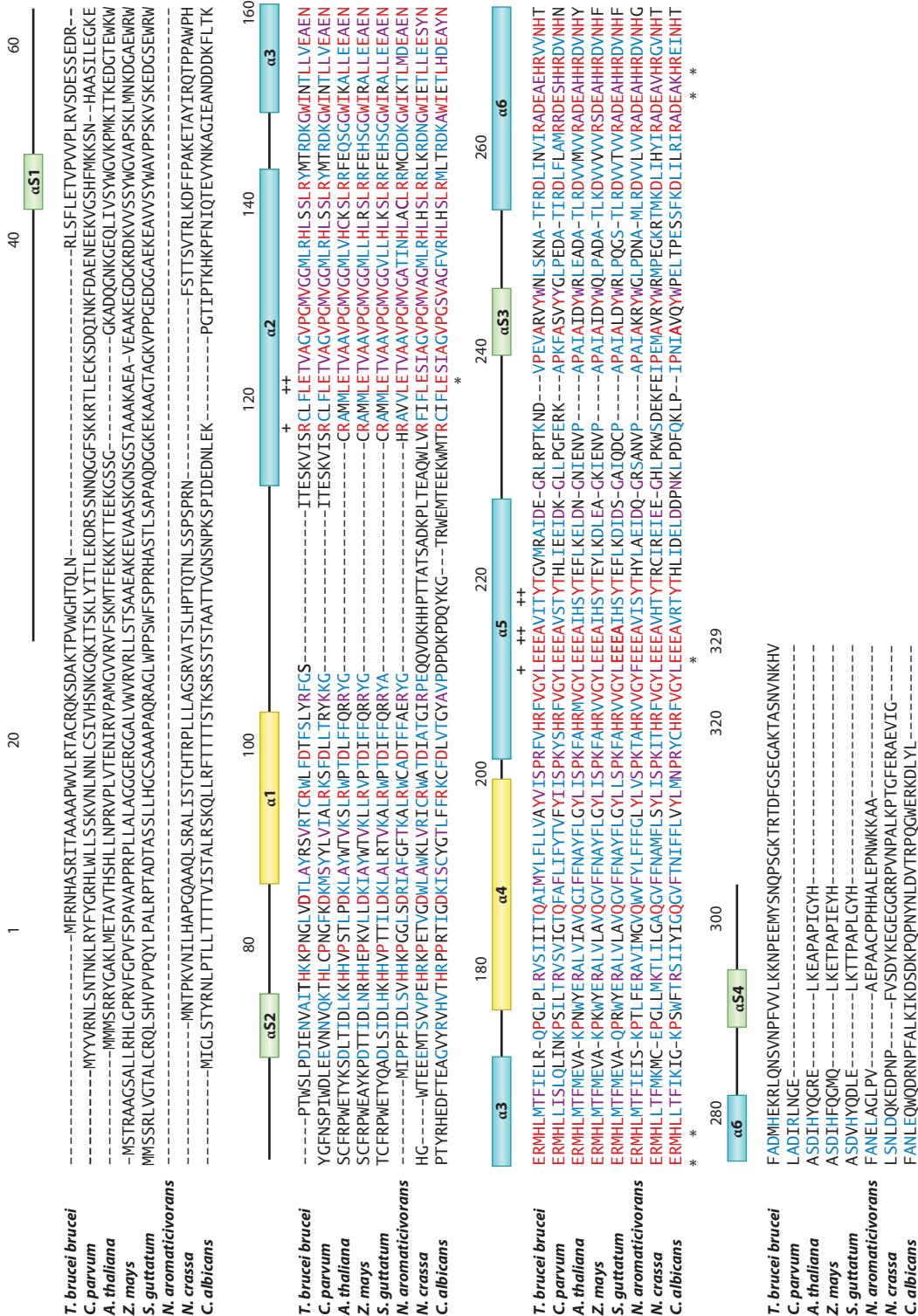
approximately perpendicular to the bundle, comparable to that found in prostaglandin H synthase (96) and squalene cyclase (132), as initially predicted by Andersson & Nordlund (11) and Berthold & Stenmark (19). Helices $\alpha 2$, $\alpha 3$, and $\alpha 4$ of one monomer and $\alpha 2^*$, $\alpha 3^*$, and $\alpha 4^*$ of the other (where the asterisk denotes the helix of a neighboring monomer) build a dimer interface (**Figure 2b**). Within the dimer interface, six residues [His-138, Leu-142, Arg-143, Arg-163, Leu-166, and Gln-187 (TAO numbering; see **Figure 3**)] are universally conserved across all known AOX sequences, and eight residues (Met-131, Met-135, Leu-139, Ser-141, Arg-147, Leu-156, Arg-180, and Ile-183) are highly conserved, indicating that a dimeric structure is common to all AOXs. This is obviously in contrast to earlier suggestions that a dimeric structure is not universal (27, 51, 121, 123). The fact that the dimer interface sequence is so highly conserved also lends credence to the notion that dimer formation is not an artifact of crystallographic conditions.

Of particular importance was the finding that, even though the first 30 amino acids in the N-terminal region are not resolved in the structure owing to faint electron density, it is apparent from the crystal structure that the N-terminal arm of one monomer extends into the other monomer (**Figure 2b**), suggesting that the N-terminal region is important for dimerization. Given that the plant N-terminal

Figure 2

Structure of the trypanosomal alternative oxidase (TAO). Long helices are labeled $\alpha 1$ to $\alpha 6$. Diiron and hydroxo atoms are shown as magenta spheres. (a) Surface representation of the dimeric structure viewed roughly perpendicular (*left*) and parallel (*right*) to the helix axes. Helices are shown as ribbons. Except for the N-terminal arm, each monomer is shaped as a compact cylinder ($50 \times 35 \times 30$ Å), and there are no significant structural differences among monomers in the asymmetric unit. A large hydrophobic region is visible on one side of the dimer surface; this region is formed by $\alpha 1$ and $\alpha 4$ plus the C-terminal region of $\alpha 2$ and the N-terminal region of $\alpha 5$ from both monomers and is inserted into the membrane to approximately 14 Å. (b) Dimer interaction with the membrane. Helices $\alpha 1$ to $\alpha 6$ are associated with chain A, and helices $\alpha 1^*$ to $\alpha 6^*$ are associated with chain B (asterisks indicate helices of the neighboring monomer). (c) Location of the diiron and hydroxo atoms within the four-helix bundle of one monomer (asterisks indicate helices in chain B). (d) Structure of the active site. Diiron and hydroxo atoms are shown as spheres, and four glutamate and two histidine residues important for diiron binding are shown as green sticks. The location of the redox-active Tyr-220 within 4.7 Å of the active site is also shown as a green stick. Carbon is shown in green, nitrogen in blue, and oxygen in red. Numbering refers to the *Trypanosoma brucei* sequence. (e) Schematic representation of the active site. (f) Hydrogen bond network within the diiron active site. Solid lines show coordinate bonds to the diiron center; dashed lines show hydrogen bonds. His-165 forms hydrogen bonds with Glu-123 and Asn-161. His-269 forms hydrogen bonds with Glu-213 and Glu-162. Asn-161, which is situated in the center of the hydrogen network, forms additional hydrogen bonds with Tyr-246 and Asp-265.





regions tend to be slightly longer than those of trypanosomes, it is interesting to speculate that the redox-active cysteines are oriented in a manner that enables disulfide linkages (121).

Additional important structural information includes the finding that a large hydrophobic region is visible on one side of the dimer surface; this region is formed by helices $\alpha 1$ and $\alpha 4$ plus the C-terminal region of $\alpha 2$ and the N-terminal region of $\alpha 5$. Because this region is present in both monomers and the opposite side of the dimer surface is relatively hydrophilic, we proposed that the dimer is bound to the inner membrane via this hydrophobic region in an interfacial fashion (**Figure 2a,b**) (112). In support of this idea, basic residues are distributed along a boundary between the hydrophobic and hydrophilic regions of the dimer surface. As shown in **Figure 3**, these residues are conserved across all amino acid sequences of the membrane-bound AOXs, and their locations make them ideal candidates to interact with the negatively charged phosphate head groups on the phospholipid membranes, as previously predicted (11). Importantly, the crystal structure is consistent with the constraint identified by Berthold et al. (17)—namely, that the subunits are oriented in such a way that the hydrophobic domains of each subunit are in the membrane. Given that the N-terminal region of each monomer interacts with its neighbor, the cysteines of each monomer are likely oriented such that they can interact with one another.

Resolution of the Active Site

Previous models of the AOX active site included a hydroxo bridge between the two irons

on the basis of a lack of spectroscopic features above 340 nm and a small value of the exchange coupling constant (20, 115). Within the diiron active site, the average distance between the two irons is 3.16 Å, which is also consistent with a single hydroxo bridge (**Figure 2d**). The active site is located in a hydrophobic environment buried deep within the molecule and comprises the diiron center, four universally conserved glutamate residues, and two universally conserved histidine residues (**Figure 2d**). In addition to the hydroxo bridge, the two irons are bridged by two glutamate residues, as predicted by Andersson & Nordlund (11), and furthermore are coordinated in a bidentate fashion by two glutamate residues. This results in a five-coordinated diiron center with a distorted square pyramidal geometry (**Figure 2d**).

The most distinctive feature of the diiron active site in the crystal structure in its oxidized state, however, is that both histidine residues are too far away from the diiron center to coordinate with the two irons. At first glance, such a primary ligation sphere is not consistent with other diiron proteins. For instance, diiron active sites of soluble diiron proteins with known structures, such as Δ^4 acyl carrier protein desaturase (53), MMO (106), RNR (92), and rubrerythrin (64), are all coordinated by at least one if not two histidine residues, and hence AOX is somewhat unusual in the composition of its primary ligation sphere. However, it should be noted that not only did the reduced-minus-oxidized FTIR difference spectra of purified TAO confirm the presence of signals that could be attributed to carboxylates, but also, equally importantly, upon reduction two of these carboxylates

Figure 3

Multiple alignment of AOX amino acid sequences. This alignment was produced from eight amino acid sequences from *Trypanosoma brucei brucei*, *Cryptosporidium parvum*, *Arabidopsis thaliana*, *Zea mays*, *Sauromatum guttatum*, *Novosphingobium aromaticivorans*, *Neurospora crassa*, and *Candida albicans*. The secondary structure elements identified in the trypanosomal alternative oxidase (TAO) structure are also shown. Helices $\alpha 1$ and $\alpha 4$, which form the hydrophobic region on the AOX molecular surface and are involved in membrane binding, are shown in yellow; helices $\alpha 2$, $\alpha 3$, $\alpha 5$, and $\alpha 6$, which form the four-helix bundle accommodating the diiron center, are shown in cyan. Amino acid residues that coordinate the diiron center and those that interact with the inhibitor are indicated by asterisks and plus symbols, respectively. Red, purple, and blue letters denote residues conserved in all eight of the organisms, in six or seven of the organisms, and in four or five of the organisms, respectively.

became protonated and peaks appeared that could be attributed to histidine residues (74). The crystal structure is therefore consistent with an active site in its oxidized form that contains carboxylate ligands but not histidine ligands. The histidine residues do, however, form hydrogen bonds with Glu-123, Asn-161, Glu-162, and Glu-213. Asn-161 is at the center of a hydrogen bond network that includes Tyr-246 and Asp-265 (112). These residues are again universally conserved, and, as is the case with RNR diiron proteins, the hydrogen bond network may be important for stabilization of the active site. Additionally, within 6 Å of the diiron center, other highly conserved hydrophobic residues include Leu-122, Ala-126, Leu-212, Ala-216, and Tyr-220 (see **Table 1**).

Role of Tyrosines

In RNR, a highly conserved tyrosine (Tyr-122) plays a critical role in electron transport (108), and similar roles for tyrosines have been suggested for AOX (2). Scrutiny of **Figure 3** reveals that although there appear to be four conserved tyrosine residues, only three of these (Tyr-198, Tyr-220, and Tyr-246) are universally conserved across all amino acid sequences of membrane-bound AOXs, including the plastid AOX (75). Tyr-198 has been proposed to be involved in ubiquinol binding (85), although its mutation does not lead to a complete loss of activity (10, 29, 90) (see **Table 1**) and crystal structure analysis of TAO indicates that it is separated from the diiron center by at least 15.8 Å (**Figure 4a**). It is located on the C-terminal portion of helix $\alpha 4$ and forms a hydrogen bond with a conserved His-206 protruding from the N-terminal portion of helix $\alpha 5$. Such a position suggests that it probably stabilizes the structure of the oxidase rather than being directly involved in ubiquinol binding.

Although Tyr-246, which is located on helix $\alpha 5$, is within electron tunneling distance of the diiron center (9.7 Å) (95), it is more likely involved in the hydrogen bond network than in electron transport because it is only 3.1 Å from Asn-161 in helix $\alpha 3$ (**Figure 2f**). This notion is

also supported by the finding that Tyr-246-Ala mutants retain some activity (90), which would not be the case if the residue were essential for electron transfer. Tyr-220, however, is buried deep within the four-helix bundle, within 4.7 Å of the diiron center (**Figure 4a**), making it the most likely candidate for the amino acid radical proposed to be involved in the AOX catalytic cycle (2) (see Catalytic Mechanism for the Reduction of Oxygen to Water, below). Indeed, Tyr-220 is universally conserved across all AOXs sequenced to date (75), and mutational analyses have unequivocally demonstrated that this residue is essential for the enzymatic activity of all AOXs (7, 90).

Of particular interest is the finding that in AOX, Tyr-220 is located on helix $\alpha 5$ (**Figure 4b**), in contrast to the redox-active Tyr in RNR (**Figure 4c**). In AOX, Phe-169 is the amino acid residue equivalent to Tyr-122 in RNR based on a comparison of their structures and amino acid sequences. However, close inspection of both structures reveals that Tyr-220 (**Figure 4b**) occupies the corresponding positions of Tyr-122 in RNR (**Figure 4c**). In contrast, RNR Phe-212 occupies the position equivalent to TAO Tyr-220 in both amino acid sequence and structure. As shown in **Figure 4**, the complementary positions of the two amino acid residues found in AOX (**Figure 4b**) and RNR (**Figure 4c**) are also observed in bacterioferritin (Tyr-58 and Leu-101; **Figure 4d**) and rubrerythrin (Leu-60 and Tyr-102; **Figure 4e**). It is interesting to speculate on whether the position change of Tyr-220 in AOX (**Figure 4b**) deep within the hydrophobic core of the protein renders it much more resistant (78, 142) to the antiproliferative effects of agents such as nitric oxide (21) in contrast to the susceptibility of RNR (class 1a and 1b) to this agent (42). The fact that the RNR in *Chlamydia* lacks the stable tyrosine radical site and is insensitive to nitric oxide supports this suggestion (54).

Ubiquinol-Binding Sites

In addition to containing an active site for the reduction of oxygen to water, AOX must

Table 1 Roles, locations, and effect of mutation of universally conserved AOX residues

SgAOX numbering	TbAOX numbering	Role	Helix number	Respiratory inhibition (%)
Leu-177	Leu-122	Substrate-binding channels 1 and 2	$\alpha 2$	61
Glu-178	Glu-123	*Fe-Fe ligand; substrate-binding channels 1 and 2	$\alpha 2$	100
Ala-181	Ala-126	*Substrate-binding channels 1 and 2	$\alpha 2$	ND
Pro-184	Pro-129	Substrate-binding channel 2	$\alpha 2$	ND
Gly-185	Gly-130	Forms kink in helix $\alpha 2$ (with P129)	$\alpha 2$	ND
Val-187	Val-132	Hydrophobic interaction with helix $\alpha 6$	$\alpha 2$	ND
His-193	His-138	Membrane-binding region/dimer interface	$\alpha 2$	62
Arg-198	Arg-143	Membrane-binding region/dimer interface	$\alpha 2$	ND
Trp-206	Trp-151	Hydrophobic interaction with helix $\alpha 6$	$\alpha 3$	95
Iso-207	Iso-152	Dimer interface	$\alpha 3$	ND
Leu-210	Leu-155	Dimer interface	$\alpha 3$	ND
Glu-213	Glu-158	*Substrate-binding channels 1 and 2	$\alpha 3$	90
Asn-216	Asn-161	*Secondary ligation sphere; hydrogen bond network	$\alpha 3$	90
Glu-217	Glu-162	*Fe-Fe ligand	$\alpha 3$	100
Arg-218	Arg-163	Membrane-binding region	$\alpha 3$	ND
Met-219	Met-164	Dimer interface; interaction with N-terminal arm	$\alpha 3$	ND
His-220	His-165	*Fe-Fe ligand	$\alpha 3$	100
Leu-221	Leu-166	Dimer interface	$\alpha 3$	ND
Pro-230	Pro-175	Dimer interface	—	ND
Gln-242	Gln-187	Dimer interface	$\alpha 4$	94
Tyr-253	Tyr-198	Dimer interface; hydrogen bonds to His-206	$\alpha 4$	53
His-261	His-206	Membrane-binding region	$\alpha 5$	98
Gly-265	Gly-210	Forms kinks in helix $\alpha 5$	$\alpha 5$	ND
Glu-268	Glu-213	*Fe-Fe ligand	$\alpha 5$	100
Glu-269	Glu-214	Interacts with N-terminal arm	$\alpha 5$	ND
Ala-271	Ala-216	*Substrate-binding channel 2	$\alpha 5$	92
Tyr-275	Tyr-220	*Catalytic cycle	$\alpha 5$	100
Ala-295	Ala-243	Hydrophobic interaction with helix $\alpha 3$	$\alpha S3$	ND
Tyr-299	Tyr-246	Secondary ligation sphere; hydrogen bond networks	$\alpha S3$	ND
Arg-316	Arg-263	Interaction with helix $\alpha 5$ and N-terminal arm	$\alpha 6$	ND
Asp-318	Asp-265	*Secondary ligation sphere; hydrogen bond network	$\alpha 6$	ND
Glu-319	Glu-266	*Fe-Fe ligand	$\alpha 6$	100
His-322	His-269	*Fe-Fe ligand	$\alpha 6$	100
Asn-326	Asn-273	Interaction with helix $\alpha 5$	$\alpha 6$	ND
His-327	His-274	Interaction with helix $\alpha 5$	$\alpha 6$	ND

Residue numbering refers to either *Sauromatum guttatum* or *Trypanosoma brucei* AOXs (SgAOX and TbAOX, respectively). Asterisks denote residues within 6 Å of the iron atoms. Helix number refers to the numbering of the α -helices given in **Figure 3**. Data expressed in the “respiratory inhibition (%)” column refer to respiratory inhibition as a result of mutation of the respective residue to Ala compared with wild-type rates and are from References 6–8, 10, 20, 29, 44, 90, and 112. ND, no data.

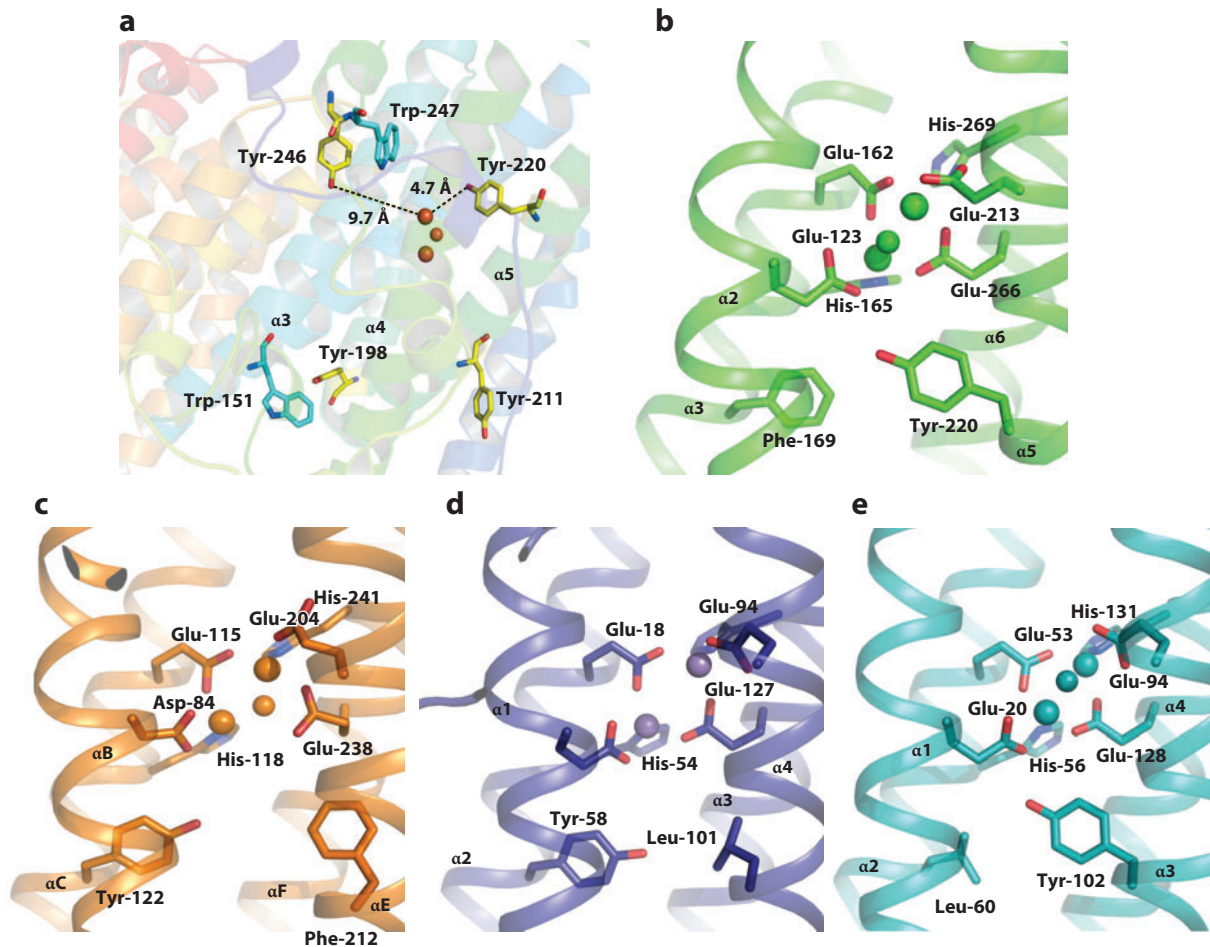


Figure 4

Locations of conserved tryptophan and tyrosine residues and comparison of diiron active sites in AOX with those in other diiron carboxylate proteins. (a) Locations of highly conserved tryptophan (cyan sticks) and tyrosine (yellow sticks) residues within the AOX four-helix bundle. Dotted lines represent distances between Tyr-246 and Tyr-220 and the diiron atoms (Fe1). The other panels show the diiron active sites of (b) AOX (green), (c) the R2 subunit of ribonucleotide reductase (orange), (d) bacterioferritin (purple), and (e) rubrerythrin (cyan). Oxygen and nitrogen atoms are shown in red and blue, respectively. Diiron, hydroxo, and oxo atoms are shown as colored spheres. Numbering refers to the *Trypanosoma brucei* sequence.

contain a binding site for ubiquinol, the reducing substrate of the protein. Although the structures of several ubiquinone-binding proteins have been determined to atomic resolution (1, 60, 141), the general architecture of this site remains elusive. Despite this, several characteristics thought to be important for ubiquinone binding have been identified. Elucidation of the ubiquinone-binding site in the membrane-associated cytochrome bc_1

complex has resulted in a model comparable to ubiquinone-binding sites in photosynthetic reaction centers in which the ubiquinone-binding pocket is formed by the ends of two transmembrane helices, thus placing the ubiquinone ring near the membrane interface (1, 114). Aromatic residues identified close to ubiquinone-binding regions may interact with the ubiquinone head group in a parallel stacking manner. Additionally, a novel ubiquinone-binding

domain containing a group of polar residues exposed to the membrane interior has been observed that appears to be uniquely conserved among ubiquinol oxidases (1). Furthermore, a sequence analysis of respiratory and photosynthetic complexes that react with ubiquinones identified a putative ubiquinone-binding motif consisting of a histidine-arginine pair and a triad element (41). In addition to these residues (41), serine, arginine, and tyrosine residues have also been identified by biochemical means as being critical for ubiquinone binding in succinate:ubiquinone oxidoreductase (56, 119, 138).

A knowledge of AOX ubiquinol-binding sites is important because they offer the potential of a novel target site for the design of specific inhibitors (104). For instance, in recent years agricultural fungal control has resulted in the development of fungicides specifically targeted to the ubiquinol-oxidation site (Q_o) of the fungal cytochrome bc_1 complex (104). One important group of Q_o site inhibitors that have proved effective in controlling plant pathogens is the strobilurin fungicides, the most widely used of which is azoxystrobin (13). Unfortunately, resistance to this fungicide often develops, making continued application ineffective (71, 135). Although the mechanism for conferring resistance to Q_o fungicides is still controversial (38, 39, 135), there is good evidence to suggest that the addition of inhibitors such as azoxystrobin to fungal pathogens results in a strong induction of AOX (135). Whether the development of AOX can account for field resistance to strobilurins is debatable; nevertheless, it is interesting to speculate on whether inhibition of AOX activity in fungal pathogens increases the sensitivity to commercially available fungicides. Although salicylhydroxamic acid (SHAM) has previously been shown to be ineffective at controlling fungicide resistance when used alongside strobilurin fungicides (13), it should be recognized that SHAM is not specific for AOX *in vivo* and, furthermore, is a poor inhibitor compared with the antibiotic ascofuranone. Ascofuranone is a ubiquinone analog isolated

from the pathogenic fungus *Ascochyta viciae* that specifically inhibits TAO at subnanomolar concentrations (82, 136, 137). For the future development of AOX-specific inhibitors similar to ascofuranone, therefore, a knowledge of AOX ubiquinone-binding sites is critical.

When the plant AOX sequence was initially mapped onto the structure of the Δ^9 -desaturase protein, a hydrophobic crevice that reaches down to the diiron center was formed; this crevice was tentatively assigned as a ubiquinol-binding site (11) because a comparable crevice was observed when RNR was used as a template for the oxidase. Such information has been used to model the AOX ubiquinol-binding site (9–11, 17, 89), thereby identifying a hydrophobic pocket between helices $\alpha 1$ and $\alpha 4$ [helices I and III in the Andersson & Nordlund model (11)] that could act as a channel enabling the substrate to gain access to the active site from the membrane-binding domain. Furthermore, the crevice also contained residues, identified in a mutagenesis screen, that result in increased resistance to the presumed competitive inhibitor SHAM (16). Interestingly, these residues flank the extremely well conserved histidine-arginine dyad (41). A number of key residues within this hydrophobic crevice were identified (10) that appeared to be critical for activity, including Tyr-199, Ser-201, His-206, and Arg-207 in addition to Tyr-220, the majority of which are highly conserved. Such mutations suggested that, in addition to the size of the amino acid chain, the presence of hydroxyl, guanidino, imidazole and aromatic groups, and polar and charged residues is important for ubiquinone binding.

An inhibitor-binding pocket was also identified in the TAO crystal structure at 2.6 Å (112) following soaking of the protein in a cryoprotectant solution supplemented with an ascofuranone derivative (**Figure 5a**). Importantly, the binding pocket is located near the membrane surface between helices $\alpha 1$ and $\alpha 5$ and is lined by 12 highly conserved residues, mutation of which leads to complete loss of enzyme activity. The aromatic head is within 4 Å of the diiron site and is surrounded

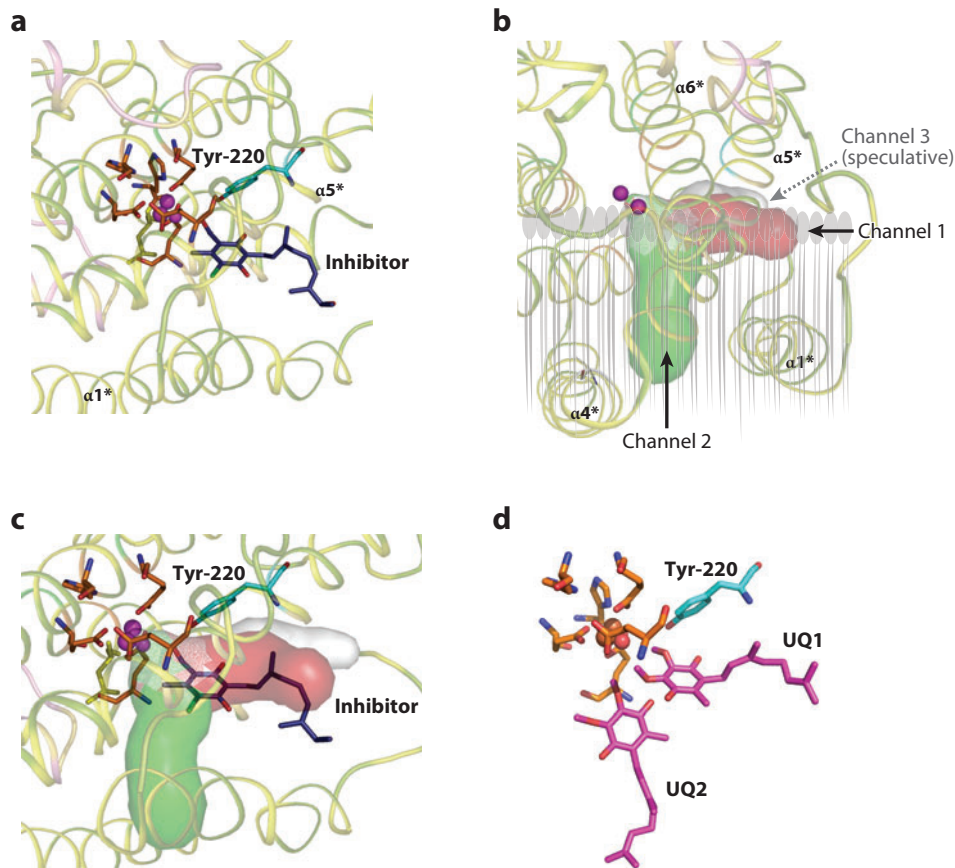


Figure 5

Locations of inhibitor and putative ubiquinol channels in AOX. (a) Locations of the diiron active site, Tyr-220, and the inhibitor within the four-helix bundle of a single monomer (asterisks indicate helices associated with chain B). (b) Channels connecting the diiron center and the AOX molecular surface, based on a search of the channels conducted using CAVER visualization software (76). A hydrophobic channel (channel 1, red) that connects the membrane lipid surface with the diiron core is located between helices $\alpha 1^*$ and $\alpha 5^*$ (chain B). Another hydrophobic channel (channel 2, green) that connects channel 1 with the membrane hydrophobic core at the diiron center is located between helices $\alpha 1^*$ and $\alpha 4^*$. A more speculative hydrophilic channel (channel 3, gray) that connects the diiron center with the protein surface (and is possibly the site of oxygen entry and water exit) is also shown. (c) Location of the inhibitor within channel 1 (red) based on the structure at 2.6 Å. This binding pocket is located near the membrane surface between helices $\alpha 1^*$ and $\alpha 5^*$, within 4 Å of the diiron center. (d) Model of two ubiquinol molecules within channels 1 and 2. Numbering refers to the *Trypanosoma brucei* sequence.

by hydrophobic residues, including Leu-122, Glu-123, Glu-213, Glu-215, Tyr-220, and Glu-266, whereas the isoprenoid tail is surrounded by hydrophilic residues.

In addition to the inhibitor-binding pocket, the CAVER visualization software (76) estimated that there are three possible entrance

channels. Channel 1 (Figure 5b), located close and approximately parallel to the membrane surface, links the AOX molecular surface with the diiron center and is the site of the inhibitor-binding pocket. Channel 2 connects channel 1 with the membrane hydrophobic core at the diiron center. The software also suggested the

presence of a third, much more highly speculative hydrophilic channel that links the diiron center with the protein surface and is possibly the site of oxygen entry and water exit. Channel 2 corresponds to the hydrophobic crevice modeled by Andersson & Nordlund (11) and is lined by some of the same suggested residues. The estimated length and diameter of channel 2 (approximately 16 and 5 Å, respectively) are comparable to previous estimates (11), and as indicated in **Figure 5d**, modeling suggests that it can accommodate ubiquinone. Channel 1 is also of sufficient length and width (13.5 and 4 Å, respectively) to bind ubiquinone, and hence is proposed to be a second substrate-binding pocket. Importantly, residues lining both channels are highly conserved with mutation, particularly of those surrounding the diiron center, resulting in >90% inhibition of activity (112).

Roles and Locations of Universally Conserved Residues

Analysis of multiple sequence alignments has revealed that the four-helix core contains 29 universally conserved residues (**Figure 3**) in addition to the six coordinating ligands (17, 40, 75); **Table 1** summarizes their roles, locations, and effects of mutations. Note that, as mentioned above, mutation of any of the six iron ligands results in complete inhibition of activity (6, 7, 9, 20, 44, 90). Helix $\alpha 2$ contains seven conserved residues in addition to an iron ligand, three of which play a role in substrate binding (Leu-122, Ala-126, and Pro-129) and two of which are important for the membrane-binding region and dimer interface, respectively (His-138 and Arg-143). The roles of Gly-130 and Val-132 are functionally less clear but nevertheless structurally important. Apart from Glu-123, only Ala-126 is within 6 Å of the active site.

Helix $\alpha 3$ contains eight conserved residues in addition to two of the iron ligands. Ile-152, Leu-155, Met-164, and Leu-166 are located within the dimer interface, whereas Arg-163 is in the membrane-binding region. Glu-158 is important for both substrate-binding cavities, whereas Asn-161 is part of the hydrogen

bond network and located within the secondary ligation sphere. Trp-151 is involved in a hydrophobic interaction with helix $\alpha 6$ through stacking with Phe-276. Two of these residues—Glu-158 and Asn-161—are within 6 Å of the active site, and mutation of either of these or mutation of Trp-151 results in almost complete loss of activity (**Table 1**).

Helix $\alpha 4$ —which, similarly to helix $\alpha 1$, is embedded within the inner membrane—contains two conserved residues, Gln-187 and Tyr-198, both of which reside at the dimer interface. We have previously suggested (10) that both of these residues are involved in ubiquinone binding, but scrutiny of the crystal structure has revealed that both are located at the dimer interface/membrane-binding region and that Tyr-198 (on helix $\alpha 4$) interacts with His-206 on helix $\alpha 5$. Mutation of either residue results in significant inhibition, probably as a result of the breakdown of helix-helix interaction (10, 85).

Helix $\alpha 5$ contains four highly conserved residues in addition to His-206 and Glu-213: Gly-210, which forms a kink in helix $\alpha 5$; Glu-214, which interacts with the N-terminal arm; Ala-216, which is a key component of the substrate-binding cavity; and, of course, Tyr-220, the universally conserved tyrosine that plays a critical role in electron transport. Both Ala-216 and Tyr-220 are within 6 Å of the active site. Small helix $\alpha 3$ contains two conserved residues: Ala-243, a residue involved in a hydrophobic interaction with helix $\alpha 3$, and Tyr-246, a key residue in the hydrogen bond network. Helix $\alpha 6$ contains four conserved residues, three of which (Arg-263, Asn-273, and His-274) are important for interhelical interaction between helices $\alpha 5$ and $\alpha 6$ and the fourth of which (Asp-265) is part of the secondary ligation sphere and hydrogen bonds with His-269.

In addition to the universally conserved residues, other critical amino acids that are conserved across the majority of species include Arg-95 and Asp-99 (both in helix $\alpha 1$); Arg-118 (in helix $\alpha 2$); Val-209, Glu-215, and Thr-221 (all in helix $\alpha 5$); Trp/Tyr-247 (in helix

α 3); and Glu-258 (in helix α 6). Arg-95, Glu-99, and Arg-118 are located within channel 1 and are probably involved in binding the substrate/inhibitor tail. Tyr-246 forms part of the hydrogen bond network linking with Asn-161. Glu-215 has previously been demonstrated to be important for catalytic activity, and although it had originally been proposed to be a member of the primary ligation sphere (8), it is apparent from the crystal structure that it is a key residue within the inhibitor-binding pocket.

Catalytic Mechanism for the Reduction of Oxygen to Water

A considerable number of diiron proteins, including Δ^9 -desaturase, MMO, RNR, and rubrerythrin, can reduce oxygen to water as a side reaction to their main respective catalytic activities (43). Gomes et al. (50) suggested that the widespread reactivity of diiron proteins toward oxygen stems from such proteins originating by divergence from a common ancestor whose possible role was an oxygen reductase. Unlike other diiron proteins, however, AOX retains that function, which it carries out through a four-electron reduction of oxygen to water. Although there is considerable experimental evidence in favor of this reaction (2, 74, 84, 85), Bhate & Ramasarma (22) recently suggested that the product of oxygen reduction is actually hydrogen peroxide and not water (i.e., a two-electron reduction process). The fact that even the simplest of diiron proteins, such as rubrerythrin, can reduce oxygen to water rather than hydrogen peroxide—as evidenced by the lack of sensitivity of its activity to catalase and/or superoxide dismutase (50)—does suggest that such a function was a characteristic in the common ancestor of the four-helix diiron protein (86). Hence it is extremely unlikely that AOX, whose ancestor probably derived from the early diiron proteins, has not retained the ability to completely reduce oxygen to water.

Several mechanistic models have been proposed to account for the net oxidation of ubiquinol and the four-electron reduction of

oxygen to water by AOX (2, 3, 17, 74). In all of these models, the first step in the catalytic cycle is generally considered to be the binding of oxygen to the diferrous state, which is generally the case for metalloenzymes reacting with oxygen (43, 116). **Figure 6** shows a scheme of the proposed cycle, based on those proposed for MMO (43) and cytochrome *c* oxidase (116, 133).

In this scheme, we propose that the diferrous state is monohydroxo bridged. Before AOX can react with oxygen, the resting oxidized state must undergo a two-electron reduction (probably by ubiquinol) to generate the diferrous center. FTIR studies (74) suggest that a carboxylate shift occurs simultaneously with the generation of this state. We propose that upon binding of oxygen to the diferrous center, two short-lived intermediates are formed prior to the formation of the peroxodiiron species, similar to the reactions observed in other systems (43, 111). The first electron, which is transferred from the diiron core, forms a superoxo species (Fe-O-O*⁻; reaction 1 in the figure) that is immediately reduced to a hydroperoxo intermediate (reaction 2) following the transfer of a proton and electron from a bound ubiquinol, thereby generating a bound ubisemiquinone. This reaction may also be accompanied by a carboxylate shift. Following these transfers, the diiron core rearranges to form a peroxodiiron species, losing water in the process (reaction 3). Homolytic cleavage of the O-O bond (reaction 4) results in an oxodiiron species following extraction of a proton and electron from Tyr-220, thereby generating a tyrosyl radical. The tyrosyl radical is re-reduced by the ubisemiquinone formed in reaction 2. It should be noted that this is one of many possible diiron core arrangements that the diiron site could exist in following the breaking of the O-O bond. The oxodiiron species, which we propose is the resting state, is then reduced by a second ubiquinol, thereby regenerating the diferrous state with the loss of water (reaction 5).

The redox cycle presented in **Figure 6** differs from previous models (2, 116) in that it does not envisage the formation of high-valent

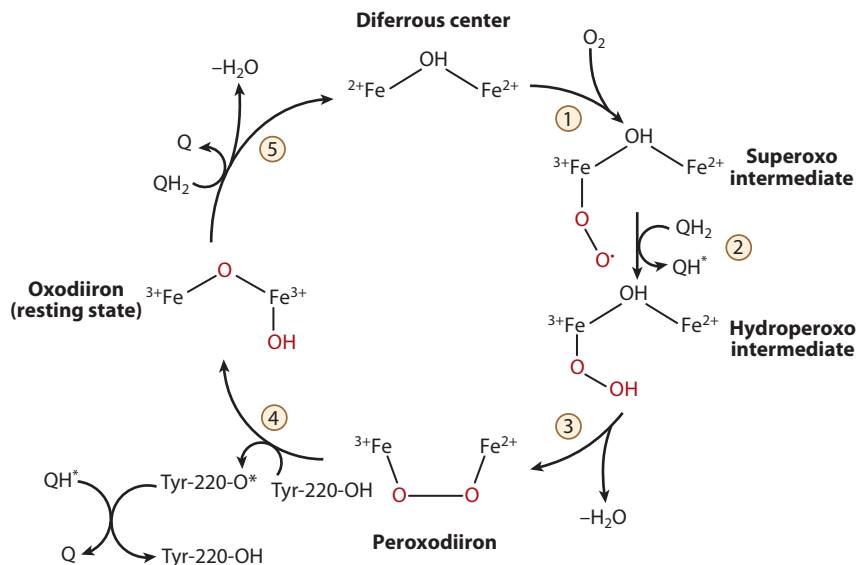


Figure 6

Mechanistic representation of a proposed AOX $O_2/2H_2O$ redox cycle. The binding of oxygen to the diferrous center (reaction 1) results in the formation of two short-lived intermediate species. The diiron core rearranges to form a peroxodiiron species (reaction 3), and following homolytic cleavage of the O-O bond (reaction 4) produces an oxodiiron species as a result of extraction of a proton and electron from Tyr-220. The tyrosyl radical is re-reduced by the ubisemiquinone formed in reaction 2. The oxodiiron species is then reduced by a second ubiquinol, thereby regenerating the diferrous state (reaction 5). (For full details, please refer to the text.)

intermediates but does involve tyrosyl and ubiquinol radicals. Such a model is consistent with the following experimental evidence:

1. The generation of a mixed-valent Fe(II)/Fe(III) EPR signal observed (20) following the introduction of molecular oxygen to a fully reduced sample [interestingly, it was estimated that the mixed-valent state accumulates to a maximum of approximately 5% of the estimated concentration of the AOX monomer (20), which compares favorably with published estimates (111)]
2. The occurrence of a carboxylate shift (74) following the two-electron reduction of the oxodiiron species to form the diferrous state (consistent with reaction 5)
3. The location of Tyr-220 in a catalytically active position (within 6 Å of the bimetallic active site) in the crystal structure (112) and the fact that this residue is universally conserved across AOX species and is essential for catalytic activity (consistent with reaction 4)
4. The fact that a Thr-179-Ala mutant (corresponding to the trypanosomal Thr-124) results in an AOX with reduced catalytic activity and increased apparent K_m for oxygen (29), which, importantly, traps a ubisemiquinone (consistent with reaction 2) (P. Heathcote & A.L. Moore, unpublished results)
5. The inclusion of a single hydroxo bridge and two ubiquinol-binding sites, as predicted from the crystal structure
6. The loss of a sharp negative band at $1,554\text{ cm}^{-1}$ observed by FTIR following the introduction of oxygen to a fully reduced AOX sample, which could arise from the loss of a tyrosyl radical (74) (such a scheme also accounts for short-lived radicals on the basis that ubisemiquinone

BN-PAGE: blue native polyacrylamide gel electrophoresis

Supercomplex: a multienzyme complex involved in substrate channeling, catalytic enhancement, and the sequestration of reactive intermediates

CysI and CysII: conserved cysteine residues equivalent to Cys-122 and Cys-172 in *Sauromatum guttatum* AOX numbering

generated in reaction 2 rapidly reduces the tyrosyl radical formed in reaction 4)

7. A low-field EPR signal with g values of approximately 16 and a line shape and amplitude comparable to those observed in other diiron proteins (20, 88)
8. The non-proton-pumping nature of AOX

NATIVE STRUCTURE OF AOX IN THERMOGENIC PLANTS

Blue native polyacrylamide gel electrophoresis (BN-PAGE) analyses have shown that thermogenic organs of *Arum maculatum* and *Symplocarpus renifolius* contain higher amounts of supercomplex I + III₂ (65, 118) compared with organs in nonthermogenic plants (36). Supercomplex I + III₂ would be beneficial to substrate channeling of the cytochrome c oxidase pathway, which contributes to oxidative phosphorylation in mitochondria; however, it may reduce the access of AOX to the complex I-mediated reduced ubiquinone.

Interestingly, Kakizaki et al. (65) recently showed that AOX from thermogenic *A. maculatum* and *S. renifolius* appears as a 150–350-kDa signal on two-dimensional BN-PAGE. Although there are few data on the mitochondrial proteins that interact with AOX, it is possible that AOX, which presumably exists as a multicomplex, primarily catalyzes reducing equivalents from ubiquinone reductases such as alternative NAD(P)H dehydrogenases (65). Based on another recent study, it appears that plant respiratory supercomplexes are affected by the intracellular environment, including oxygen availability and the pH of the mitochondrial matrix (97). Therefore, the native structure of AOX in the mitochondrial respiratory chain may be more dynamic and complex than previously considered.

POSTTRANSLATIONAL REGULATION OF AOX ACTIVITY IN THERMOGENIC PLANTS

Posttranslational regulation of AOX activity in plants is controlled by two interrelated

mechanisms: Reduction of an intermolecular disulfide bond results in a more active non-covalently linked dimer (121), and further activation of the reduced AOX occurs by the addition of α -keto acids, particularly pyruvate (80). The mechanism of α -keto acid regulation involves two conserved cysteine residues, CysI and CysII (120, 122). The N-terminal CysI acts as a site for intermolecular bond formation and α -keto acid activation (102, 131), whereas CysII has a less well defined role in α -keto acid activation. SgAOX from the thermogenic *Sauromatum guttatum* is constitutively active in the absence of pyruvate, and the glutamine, aspartic acid, and cysteine (QDC) motif of three adjacent amino acid residues plays a role in its pyruvate-insensitive activity (25, 28). In contrast, another thermogenic plant, *S. renifolius*, expresses a pyruvate-stimulated SrAOX that possesses the glutamine, asparagine, and valine (ENV) motif instead of the QDC motif (94) (see residues 232–235 in **Figure 3**).

The glutamic acid/aspartic acid, asparagine, and valine (E/DNV) motif may be crucial during pyruvate activation in nonthermogenic plants (28). Recent analysis of *AmAOX1e*, one of the seven cDNAs for *A. maculatum* AOX that is abundantly expressed in thermogenic appendices, indicates that the ENV motif is substituted by the glutamine, asparagine, and threonine (QNT) motif, although CysI and CysII residues are well conserved in its primary amino acid sequence (58). In particular, a yeast heterologous expression system demonstrated that *AmAOX1e* is insensitive to stimulation by pyruvate. Moreover, two *AOX* genes that lack CysI, *NnAOX1a* and *NnAOX1b*, have been isolated from thermogenic *Nelumbo nucifera*, and these gene products may be stimulated by succinate and not by pyruvate (51). *A. maculatum* and *S. guttatum* show transient and rather uncontrolled heat production, whereas *S. renifolius* and *N. nucifera* maintain their flower temperatures. Therefore, it is tempting to speculate that the type of AOX molecule, which is characterized by the presence of a conserved CysI residue and/or E/DNV motif, is related to the phenotype of thermogenic plants.

N-TERMINAL EXTENSION AND STRUCTURAL-FUNCTIONAL CONSIDERATIONS

With the exception of CysI, the N-terminal sequences of plant AOXs are not well conserved, and this region has been considered independently from the structurally defined four-helix bundle. For instance, although the distance between CysI and CysII in AOXs from 13 different plant species is 50 amino acids, the distance between the predicted N-terminal sequence and CysI varies. However, functional regulation might occur via phosphorylation of the N-terminal extension of AOX. The Musite tool, which has been developed for global prediction of general and kinase-specific phosphorylation sites (46), predicted at least three potential phosphorylation sites in SgAOX [Ser-68, Thr-82, and Tyr-102 (SgAOX numbering)]. Because some of these amino acid residues are well conserved in both thermogenic and nonthermogenic plant AOXs, protein phosphorylation might play a role in controlling the activity through charge-induced conformational changes and/or an interaction with other mitochondrial proteins.

RETROGRADE REGULATION OF AOX

Response to mitochondrial perturbations of the nuclear gene for AOX is the most well studied mitochondria-to-nucleus signaling pathway—referred to as the retrograde

regulation system—in plants (31, 32, 52, 79, 101, 110, 129, 130). The transcription factor ABSCISIC ACID INSENSITIVE 4 (ABI4), a regulator of plastid retrograde signaling (79, 70), was first identified as a repressor of AOX1a (49). Although ABI4 seems to be one of the downstream components of a mitochondrial retrograde signaling pathway, the entire signaling cascade is still unknown.

Another regulator that may play a role in the retrograde signaling of AOX gene expression is INCREASED SIZE EXCLUSION LIMIT 2 (ISE2) (24). ISE2 was first discovered as a gene encoding a putative DEVH-box RNA helicase involved in plasmodesmata function during *Arabidopsis* embryogenesis (69). Of particular interest is that in the *ise2* mutant, genes for AOX1a and several external rotenone-insensitive alternative mitochondrial NAD(P)H dehydrogenases (NDBs) were coinduced (24). In this case, the NDBs oxidize NADH to reduce ubiquinone to ubiquinol, which is in turn oxidized by AOX1a. Kakizaki et al. (65) showed that in *A. maculatum*, not only AOX gene expression but also the NDB transcript and protein levels are significantly higher in thermogenic appendices. Such coordinated gene expression for AOX1a and NDBs also contributes to an energy-dissipating system in thermogenic plants, and ISE2 should be one of the future target genes for a deeper understanding of retrograde regulation of AOX in plants.

ISE2: INCREASED SIZE EXCLUSION LIMIT 2

DEVH box: a motif found in RNA helicase

NDB: external rotenone-insensitive NAD(P)H dehydrogenase

SUMMARY POINTS

1. The cyanide- and antimycin-A-resistant AOX is a diiron carboxylate protein that is located on the substrate side of the mitochondrial respiratory chain, is non-protonmotive, and results in the net oxidation of ubiquinol and the reduction of oxygen to water.
2. Crystallographic studies have revealed that AOX is a homodimer, with each monomer comprising six long and four short α -helices arranged in an antiparallel fashion, thereby forming a four-helix bundle that acts as a scaffold to bind the two iron atoms.
3. In AOX's oxidized state, the two iron atoms within each active site are linked by a hydroxo bridge and ligated by four highly conserved glutamate residues.

4. A highly conserved tyrosine residue plays a key role in the catalytic cycle, and we propose a catalytic cycle to account for the four-electron reduction of oxygen to water, which involves several short-lived intermediates and radical species.
5. In addition to the classical conserved CysI residues, plant AOX sequences contain an E/DNV or QDC motif that appears to play a role in the posttranslational regulation of activity, the presence of which could be related to the phenotype of thermogenic plants.
6. Mitochondrial retrograde regulation involves coordinated gene expression of AOX and several external alternative mitochondrial NDBs.

FUTURE ISSUES

1. Crystal structures of other AOX proteins are needed to determine whether a homodimeric structure is universal. Information on the N-terminal region is of particular importance because the current structure indicates that the N-terminal region of each monomer is intimately associated with its neighbor and probably plays a key regulatory role in altering the conformation of the four-helix bundle.
2. It is important to obtain structures of both wild-type and mutant forms of AOX in a reduced state to determine whether the reduction results in carboxylate shifts, thereby changing the conformation and primary ligation sphere of the diiron center.
3. Further spectroscopic studies are needed to confirm the role of tyrosine in the catalytic cycle. Such studies should reveal whether short-lived radical species are generated during the turnover of the cycle. The use of mutants, which have altered turnover rates, may prove important in trapping such intermediates.
4. More information is needed on the native structure of AOX, in particular its interaction with other mitochondrial components and the extent to which these interactions are governed by various physiological conditions.
5. Exploring the mechanisms of AOX turnover should reveal the mitochondrial proteases that digest AOX and the possible involvement of the retrograde signaling pathway(s) specifically induced by degradation products.

DISCLOSURE STATEMENT

The authors are not aware of any affiliations, memberships, funding, or financial holdings that might be perceived as affecting the objectivity of this review.

ACKNOWLEDGMENTS

This work was supported in part by Grant-in-Aid for Scientific Research on Priority Areas 18073004 (to K.K.) and Grant-in-Aid for Scientific Research (B) 24380182 (to K.I.) from the Japanese Society for the Promotion of Science, and by the Targeted Proteins Research Program (to K.K. and S.H.) of the Japanese Ministry of Education, Science, Culture, Sports, and Technology (MEXT). A.L.M. gratefully acknowledges the Biotechnology and Biological Sciences Research Council for financial support and (with K.K.) the Prime Minister's Initiative 2 (Connect—British Council) fund for collaborative twinning.

LITERATURE CITED

1. Abramson J, Riistama S, Larsson G, Jasaitis A, Svensson-Ek M, et al. 2000. The structure of the ubiquinol oxidase from *Escherichia coli* and its ubiquinone binding site. *Nat. Struct. Biol.* 7:910–17
2. Affourtit C, Albury MS, Crichton PG, Moore AL. 2002. Exploring the molecular nature of alternative oxidase regulation and catalysis. *FEBS Lett.* 510:122–26
3. Affourtit C, Albury MS, Moore AL. 2000. The active site of the plant alternative oxidase: structural and mechanistic considerations. *Pest. Manag. Sci.* 56:31–38
4. Affourtit C, Krab K, Moore AL. 2001. Control of plant mitochondrial respiration. *Biochim. Biophys. Acta* 1504:58–69
5. Affourtit C, Moore AL. 2004. Purification of the plant alternative oxidase from *Arum maculatum*: measurement, stability and metal requirement. *Biochim. Biophys. Acta* 1608:181–89
6. Ajayi WU, Chaudhuri M, Hill GC. 2002. Site-directed mutagenesis reveals the essentiality of the conserved residues in the putative diiron active site of the trypanosome alternative oxidase. *J. Biol. Chem.* 277:8187–93
7. Albury MS, Affourtit C, Crichton PG, Moore AL. 2002. Structure of the plant alternative oxidase site-directed mutagenesis provides new information on the active site and membrane topology. *J. Biol. Chem.* 277:1190–94
8. Albury MS, Affourtit C, Moore AL. 1998. A highly conserved glutamate residue (E270) is essential for plant alternative oxidase activity. *J. Biol. Chem.* 273:30301–6
9. Albury MS, Elliott C, Moore AL. 2009. Towards a structural elucidation of the alternative oxidase in plants. *Physiol. Plant.* 137:316–27
10. Albury MS, Elliott C, Moore AL. 2010. Ubiquinol-binding site in the alternative oxidase: Mutagenesis reveals features important for substrate binding and inhibition. *Biochim. Biophys. Acta* 1797:1933–39
11. Andersson ME, Nordlund P. 1999. A revised model of the active site of alternative oxidase. *FEBS Lett.* 449:17–22
12. Arcangeli G. 1879. L'Amorphophallus titanum Beccari. *J. Bot. Soc. Ital.* 11:217–23
13. Bartlett DW, Clough JM, Goodwin JR, Hall AA, Hammer M, et al. 2002. The strobilurins fungicides. *Pest. Manag. Sci.* 58:649–62
14. Behan RK, Lippard SJ. 2010. The aging-associated enzyme CLK-1 is a member of the carboxylate-bridged diiron family of proteins. *Biochemistry* 49:9679–81
15. Bendall DS, Bonner WD Jr. 1971. Cyanide-insensitive respiration in plant mitochondria. *Plant Physiol.* 47:236–45
16. Berthold DA. 1998. Isolation of mutants of the *Arabidopsis thaliana* alternative oxidase (ubiquinol: oxygen oxidoreductase) resistant to salicylhydroxamic acid. *Biochim. Biophys. Acta* 1364:73–83
17. Berthold DA, Andersson ME, Nordlund P. 2000. New insight into the structure and function of the alternative oxidase. *Biochim. Biophys. Acta* 1460:241–54
18. Berthold DA, Siedow JN. 1993. Partial purification of the cyanide-resistant alternative oxidase of skunk cabbage (*Symplocarpus foetidus*) mitochondria. *Plant Physiol.* 101:113–19
19. Berthold DA, Stenmark P. 2003. Membrane-bound di-iron carboxylate proteins. *Annu. Rev. Plant Biol.* 54:497–517
20. Berthold DA, Voevodskaya N, Stenmark P, Gräslund A, Nordlund P. 2002. EPR studies of the mitochondrial alternative oxidase: evidence for a diiron carboxylate center. *J. Biol. Chem.* 277:43608–14
21. Besson-Bard A, Pugin A, Wendehenne D. 2008. New insights into nitric oxide signalling in plants. *Annu. Rev. Plant Biol.* 59:21–39
22. Bhate RH, Ramasarma T. 2009. Evidence for H₂O₂ as the product of reduction of oxygen by alternative oxidase in mitochondria from potato tubers. *Arch. Biochem. Biophys.* 486:165–69
23. Bonner WD, Clarke SD, Rich PR. 1986. Partial purification and characterization of the quinol oxidase activity of *Arum maculatum* mitochondria. *Plant Physiol.* 80:838–42
24. Burch-Smith TM, Brunkard JO, Choi YG, Zambryski PC. 2011. Organelle-nucleus cross-talk regulates plant intercellular communication via plasmodesmata. *Proc. Natl. Acad. Sci. USA* 108:1451–60
25. Carré JE, Crichton PG, Affourtit C, Albury MS, Moore AL. 2011. Interaction of purified plant alternative oxidase from *Arum maculatum* with pyruvate. *FEBS Lett.* 585:397–401

26. Caspary R. 1855. Über warmentwicklung in der bluthe der *Victoria regia*. *Monatsber. Königl. Preuss. Akad. Wiss. Berlin* 3:711–56
27. Chaudhuri M, Ott RD, Saha L, Williams S, Hill GC. 2005 The *Trypanosoma* alternative oxidase exists as a monomer in *Trypanosoma brucei* mitochondria. *Parasitol. Res.* 96:178–83
28. Crichton PG, Affourtit C, Albury MS, Carré JE, Moore AL. 2005. Constitutive activity of *Sauromatum guttatum* alternative oxidase in *Schizosaccharomyces pombe* implicates residues in addition to conserved cysteines in α -keto acid activation. *FEBS Lett.* 579:331–36
29. Crichton PG, Albury MS, Affourtit C, Moore AL. 2010. Mutagenesis of the *Sauromatum guttatum* alternative oxidase reveals features important for oxygen binding and catalysis. *Biochim. Biophys. Acta* 1797:732–37
30. Del Rizzo PA, Bi Y, Dunn SD, Shilton BH. 2002. The “second stalk” of *Escherichia coli* ATP synthase: structure of the isolated dimerization domain. *Biochemistry* 41:6875–84
31. Djajanegara I, Finnegan PM, Mathieu C, McCabe T, Whelan J, et al. 2002. Regulation of alternative oxidase gene expression in soybean. *Plant Mol. Biol.* 50:735–42
32. Dojcinovic D, Krosting J, Harris AJ, Wagner D, Rhoads DM. 2005. Identification of a region of the Arabidopsis AtAOX1a promoter necessary for mitochondrial retrograde regulation of expression. *Plant Mol. Biol.* 58:159–75
33. Efremov RG, Baradaran R, Sazanov LA. 2010. The architecture of respiratory complex I. *Nature* 465:441–45
34. Elthon TE, McIntosh L. 1986. Characterisation and solubilisation of the alternative oxidase of *Sauromatum guttatum* mitochondria. *Plant Physiol.* 82:1–6
35. Elthon TE, McIntosh L. 1987. Identification of the alternative terminal oxidase of higher plant mitochondria. *Proc. Natl. Acad. Sci. USA* 84:8399–403
36. Eubel H, Jänsch L, Braun H-P. 2003. New insights into the respiratory chain of plant mitochondria. Supercomplexes and a unique composition of complex II. *Plant Physiol.* 133:274–86
37. Fato R, Cavazzoni M, Castelluccio C, Parenti Castelli G, Palmer G, et al. 1993. Steady-state kinetics of ubiquinol–cytochrome *c* reductase in bovine heart submitochondrial particles: diffusional effects. *Biochem. J.* 290:225–36
38. Fernandez-Ortuno D, Tores JA, de Vicente A, Perez-Garcia A. 2008. Field resistance to QoI fungicides in *Podosphaera fusca* is not supported by typical mutations in the mitochondrial cytochrome *b* gene. *Pest. Manag. Sci.* 62:694–702
39. Fernandez-Ortuno D, Tores JA, de Vicente A, Perez-Garcia A. 2008. Mechanisms of resistance to QoI fungicides in phytopathogenic fungi. *Int. Microbiol.* 11:1–9
40. Finnegan P, Soole KL, Umbach AL. 2004. Alternative mitochondrial electron transport proteins in higher plants. In *Plant Mitochondria: From Genome to Function*, Adv. Photosynth. Respir. 17, ed. DA Day, AH Millar, J Whelan, pp. 163–230. Dordrecht: Springer
41. Fisher N, Rich PR. 2000. A motif for quinone binding sites in respiratory and photosynthetic systems. *J. Mol. Biol.* 296:1153–62
42. Fontecave M. 1998. Ribonucleotide reductases and radical reactions. *Cell. Mol. Life Sci.* 54:684–95
43. Friedle S, Reisner E, Lippard S. 2010. Current challenges of modelling the diiron enzyme active sites for dioxygen activation by biomimetic synthetic complexes. *Chem. Soc. Rev.* 39:2768–79
44. Fu A, Park S, Rodermel S. 2005. Sequences required for the activity of PTOX (IMMUTANS), a plastid terminal oxidase: *in vitro* and *in planta* mutagenesis of iron-binding sites and a conserved sequence that corresponds to Exon 8. *J. Biol. Chem.* 280:42489–96
45. Fukai Y, Amino H, Hirawake H, Yabu Y, Ohta N, et al. 1999. Functional expression of the ascofuranone-sensitive *Trypanosoma brucei brucei* alternative oxidase in the cytoplasmic membrane of *Escherichia coli*. *Comp. Biochem. Physiol. C* 124:141–48
46. Gao J, Thelen JJ, Dunke AK, Xu D. 2010. Musite, a tool for global prediction of general and kinase-specific phosphorylation sites. *Mol. Cell. Proteomics* 9:2586–600
47. Garreau M. 1851. Mémoire sur les relations qui existent entre l’oxygène consommé par le spadice de *l’Arum italicum*, en état de paroxysme, et la chaleur qui se produit. *Ann. Sci. Nat. Bot. Ser.* 3 16:250–56
48. Gibbons C, Montgomery MG, Leslie AGW, Walker JE. 2000. The structure of the central stalk in bovine F₁-ATPase at 2.4 Å resolution. *Nat. Struct. Biol.* 7:1055–61

49. Giraud E, Van Aken O, Ho LHM, Whelan J. 2009. The transcription factor ABI4 is a regulator of mitochondrial retrograde expression of *alternative oxidase1 α* . *Plant Physiol.* 150:1286–96
50. Gomes CM, Le Gall J, Xavier AV, Teixeira M. 2001. Could a diiron-containing four-helix-bundle protein have been a primitive oxygen reductase? *Chem. Biochem.* 7:583–87
51. Grant N, Onada Y, Kakizaki Y, Ito K, Watling J, et al. 2009. Two Cys or not two Cys? That is the question; alternative oxidase in the thermogenic plant sacred lotus. *Plant Physiol.* 150:987–95
52. Gray GR, Villarimo AR, Whitehead CL, McIntosh L. 2004. Transgenic tobacco (*Nicotiana tabacum* L.) plants with increased expression levels of mitochondrial NADP⁺-dependent isocitrate dehydrogenase: evidence implicating this enzyme in the redox activation of the alternative oxidase. *Plant Cell Physiol.* 45:1413–25
53. Guy JE, Whittle E, Kumaran D, Lindqvist Y, Shanklin J. 2007. The crystal structure of the ivy D4-16:0-ACP desaturase reveals structural details of the oxidized active site and potential determinants of regioselectivity. *J. Biol. Chem.* 282:19863–71
54. Hogbom M, Stenmark P, Voevodskaya N, McClary G, Graslund A, et al. 2004. The radical site in chlamydial ribonucleotide reductase defines a new R2 subclass. *Science* 305:245–48
55. Hooker JD. 1981 *Amorpboballus titanum*: native of Sumatra. *Curtis's Bot. Mag.* 3(47):7153–55
56. Horsefield R, Yankovskaya V, Sexton G, Whittingham W, Shiomi K, et al. 2006. Structural and computational analysis of the quinone-binding site of complex II (succinate-ubiquinone oxidoreductase): a mechanism of electron transfer and proton conduction during ubiquinone reduction. *J. Biol. Chem.* 281:7309–16
57. Huq S, Palmer JM. 1978. Isolation of a cyanide-resistant duroquinol oxidase from *Arum maculatum* mitochondria. *FEBS Lett.* 95:217–20
58. Ito K, Ogata T, Kakizaki Y, Elliott C, Albury MS, et al. 2011. Identification of a gene for pyruvate-insensitive mitochondrial alternative oxidase expressed in the thermogenic appendices in *Arum maculatum*. *Plant Physiol.* 157:1721–32
59. Iwata M, Lee Y, Yamashita T, Yagi T, Iwata S, et al. 2012. The structure of the yeast NADH dehydrogenase (Ndi1) reveals overlapping binding sites for water- and lipid-soluble substrates. *Proc. Natl. Acad. Sci. USA* 109:15247–52
60. Iwata S, Lee JW, Okada K, Lee JK, Iwata M, et al. 1998. Complete structure of the 11-subunit bovine mitochondrial cytochrome bc₁ complex. *Science* 281:64–71
61. Jacoby RP, Taylor NL, Miller AH. 2011. The role of mitochondrial respiration in salinity tolerance. *Trends Plant Sci.* 16:614–23
62. James WO, Beevers H. 1950. The respiration of *Arum* spadix. A rapid respiration, resistant to cyanide. *New Phytol.* 49:353–74
63. James WO, Elliott DC. 1955. Cyanide-resistant mitochondria from the spadix of an *Arum*. *Nature* 175:89
64. Jin S, Kurtz DM Jr, Liu ZJ, Rose J, Wang BC. 2002. X-ray crystal structures of reduced rubrerythrin and its azide adduct: a structure-based mechanism for a non-heme diiron peroxidase. *J. Am. Chem. Soc.* 124:9845–55
65. Kakizaki Y, Moore AL, Ito K. 2012. Different molecular bases underlie the mitochondrial respiratory activity in the homoeothermic spadices of *Symplocarpus renifolius* and the transiently thermogenic appendices of *Arum maculatum*. *Biochem. J.* 445:237–46
66. Kay CJ, Palmer JM. 1985. Solubilization of the alternative oxidase from cuckoo-pint (*Arum maculatum*) mitochondria: stimulation by high concentrations of ions and effects of specific inhibitors. *Biochem. J.* 228:309–18
67. Kido Y, Sakamoto K, Nakamura K, Harada M, Suzuki T, et al. 2010. Purification and kinetic characterisation of recombinant alternative oxidase from *Trypanosoma brucei brucei*. *Biochim. Biophys. Acta* 1797:443–50
68. Kido Y, Shiba T, Inaoka DK, Sakamoto K, Nara T, et al. 2010. Crystallization and preliminary crystallographic analysis of cyanide-insensitive alternative oxidase from *Trypanosoma brucei brucei*. *Acta. Crystallogr. F* 66:275–78
69. Kobayashi K, Otegui MS, Krishnakumar S, Mindrinos M, Zambryski P. 2007. *INCREASED SIZE EXCLUSION LIMIT2* encodes a putative DEVH box RNA helicase involved in plasmodesmata function during *Arabidopsis* embryogenesis. *Plant Cell* 19:1885–97

70. Koussevitzky S, Nott A, Mockler TC, Hong F, Sachetto-Martins G, et al. 2007. Signals from chloroplasts converge to regulate nuclear gene expression. *Science* 316:715–19
71. Kraiczky P, Haase U, Gencic S, Flindt S, Anke T, et al. 1996. The molecular basis for the natural resistance of the cytochrome *bc*₁ complex from strobilurin-producing basidiomycetes to centre Q_P inhibitors. *Eur. J. Biochem.* 235:54–63
72. Kumar AM, Soll D. 1992. *Arabidopsis* alternative oxidase sustains *Escherichia coli* respiration. *Proc. Natl. Acad. Sci. USA* 89:10842–46
73. Lamarck JB. 1778. *Flore Française, ou description Succincte de toutes les Plantes qui croissent naturellement en France*. Vol. 3. Paris: Impr. Natl. 2nd ed.
74. Maréchal A, Kido Y, Kita K, Moore AL, Rich PR. 2009. Three redox states of *Trypanosoma brucei* alternative oxidase identified by infrared spectroscopy and electrochemistry. *J. Biol. Chem.* 284:31827–33
75. McDonald AE. 2009. Alternative oxidase: What information can protein sequence comparisons give us? *Physiol. Plant.* 137:328–41
76. Medek P, Benes P, Sochor J. 2007. Computation of tunnels in protein molecules using Delaunay triangulation. *J. WSCG* 15:107–14
77. Meeuse BJD. 1975. Thermogenic respiration in aroids. *Annu. Rev. Plant Physiol. Plant Mol. Biol.* 26:117–26
78. Millar AH, Day DA. 1996. Nitric oxide inhibits the cytochrome oxidase but not the alternative oxidase of plant mitochondria. *FEBS Lett.* 398:155–58
79. Millar AH, Whelan J, Soole KL, Day DA. 2011. Organization and regulation of mitochondrial respiration in plants. *Annu. Rev. Plant Biol.* 62:79–104
80. Millar AH, Wiskich J, Whelan J, Day DA. 1993. Organic acid activation of the alternative oxidase of plant mitochondria. *FEBS Lett.* 329:259–62
81. Minagawa N, Sakajo S, Komiyama T, Yoshimoto A. 1990. Essential role of ferrous iron in cyanide-resistant respiration *Hansenula anomola*. *FEBS Lett.* 267:114–16
82. Minagawa N, Yabu Y, Kita K, Nagai K, Ohta N, et al. 1996. An antibiotic, ascofuranone, specifically inhibits respiration and in vitro growth of long slender bloodstream forms of *Trypanosoma brucei brucei*. *Mol. Biochem. Parasitol.* 81:127–36
83. Miyake K. 1898. Some physiological observations on *Nelumbo nucifera*. *Bot. Mag. Tokyo* 12:112–17
84. Möller IM, Rasmussen AG, Siedow JN, Vanlerberghe GC. 2010. The product of the alternative oxidase is still H₂O. *Arch. Biochem. Biophys.* 495:93–94
85. Moore AL, Albury MS. 2008. Further insights into the structure of the alternative oxidase: from plants to parasites. *Biochem. Soc. Trans.* 36:1022–26
86. Moore AL, Albury MS, Crichton P, Affourtit C. 2002. Function of the alternative oxidase: Is it still a scavenger? *Trends Plant Sci.* 7:478–81
87. Moore AL, Bonner WD Jr, Rich PR. 1978. The determination of the proton motive force during cyanide insensitive respiration in plant mitochondria. *Arch. Biochem. Biophys.* 186:298–306
88. Moore AL, Carré JE, Affourtit C, Albury MS, Crichton PG, et al. 2008. Compelling EPR evidence that the alternative oxidase is a diiron carboxylate protein. *Biochim. Biophys. Acta* 1777:327–30
89. Moore AL, Umbach AL, Siedow JN. 1995. Structure-function relationship of the alternative oxidase of plant mitochondria: a model of the active site. *J. Bioenerg. Biomembr.* 27:367–77
90. Nakamura K, Sakamoto K, Kido Y, Fujimoto Y, Suzuki T, et al. 2005. Mutational analysis of the *Trypanosoma vivax* alternative oxidase: The E(X)₆Y motif is conserved in both mitochondrial alternative oxidase and plastid terminal oxidase and is indispensable for enzyme activity. *Biochem. Biophys. Res. Commun.* 334:593–600
91. Nihei C, Fukai Y, Kawai K, Osanai A, Yabu Y, et al. 2003. Purification of active recombinant trypanosome alternative oxidase. *FEBS Lett.* 538:35–40
92. Nordlund P, Eklund H. 1993. Structure and function of the *Escherichia coli* ribonucleotide reductase protein R2. *J. Mol. Biol.* 232:123–64
93. Okunuki K. 1939. Über den Gaswechsel der Pollen. II. *Acta Phytoclim.* 11:27–64

94. Onda Y, Kato Y, Abe Y, Ito T, Ito-Inaba Y, et al. 2007. Pyruvate-sensitive AOX exists as a non-covalently associated dimer in the homeothermic spadix of the skunk cabbage, *Symplocarpus renifolius*. *FEBS Lett.* 581:5852–58
95. Page CC, Moser CC, Chen X, Dutton PL. 1999. Natural engineering in principles of electron tunnelling in biological oxidation-reduction. *Nature* 402:47–52
96. Picot D, Loll PJ, Garavito RM. 1994. The X-ray crystal structure of the membrane protein prostaglandin H2 synthase-1. *Nature* 367:243–49
97. Ramírez-Aguilar SJ, Keuthe M, Rocha M, Fedyaev VV, Kramp K, et al. 2011. The composition of plant mitochondrial supercomplexes changes with oxygen availability. *J. Biol. Chem.* 286:43045–53
98. Rasmusson AG, Fernie AR, van Dongen JT. 2009. Alternative oxidase: a defence against metabolic fluctuations? *Physiol. Plant.* 137:371–82
99. Rastogi VK, Girvin ME. 1999. Structural changes linked to proton translocation by subunit *c* of the ATP synthase. *Nature* 402:263–68
100. Rhoads DM, McIntosh L. 1991. Isolation and characterization of a cDNA clone encoding an alternative oxidase protein of *Sauromatum guttatum* (Schott). *Proc. Natl. Acad. Sci. USA* 88:2122–26
101. Rhoads DM, Subbiah CC. 2007. Mitochondrial retrograde regulation in plants. *Mitochondrion* 7:177–94
102. Rhoads DM, Umbach AL, Sweet CR, Lennon AM, Rauch GS, et al. 1998. Regulation of the cyanide-resistant alternative oxidase of plant mitochondria. Identification of the cysteine residue involved in α -keto acid stimulation and intersubunit disulfide bond formation. *J. Biol. Chem.* 273:30750–56
103. Rich PR. 1978. Quinol oxidation in *Arum maculatum* mitochondria and its application to the assay, solubilisation and partial purification of the alternative oxidase. *FEBS Lett.* 96:252–66
104. Rich PR. 1996. Quinone binding sites of membrane proteins as targets for inhibitors. *Pestic. Sci.* 47:287–96
105. Rich PR, Moore AL. 1976. The involvement of the proton motive ubiquinone cycle in the respiratory chain of higher plants and its relation to the branchpoint of the alternate pathway. *FEBS Lett.* 65:339–44
106. Rosenzweig AC, Frederick CA, Lippard SJ, Nordlund P. 1993. Crystal structure of a bacterial non-haem iron hydroxylase that catalyses the biological oxidation of methane. *Nature* 366:537–43
107. Sakamoto H, Miyoshi M, Ohshima K, Kuwabara K, Kano T, et al. 1989. Role of the isoprenyl tail of ubiquinone in reaction with respiratory enzymes: studies with bovine heart mitochondrial complex I and *Escherichia coli* *bo*-type ubiquinol oxidase. *Biochemistry* 37:15106–13
108. Schmidt PP, Rova U, Katterle B, Thelander L, Gräslund A. 1998. Kinetic evidence that a radical transfer pathway in protein R2 of mouse ribonucleotide reductase is involved in generation of the tyrosyl free radical. *J. Biol. Chem.* 273:21463–72
109. Schonbaum GR, Bonner WD Jr, Storey BT, Bahr JT. 1971. Specific inhibition of the cyanide-insensitive respiratory pathway in plant mitochondria by hydroxamic acids. *Plant Physiol.* 47:126–28
110. Schwarzländer M, König A-C, Sweetlove LJ, Finkemeier I. 2012. The impact of impaired mitochondrial function on retrograde signalling: a meta-analysis of transcriptomic responses. *J. Exp. Bot.* 63:1735–50
111. Shan X, Que L Jr. 2005. Intermediates in the oxygenation of a nonheme diiron(II) complex, including the first evidence for a bound superoxo species. *Proc. Natl. Acad. Sci. USA* 102:5340–45
112. Shiba T, Kido Y, Sakamoto K, Inaoka DK, Tsuge C, et al. 2013. Structure of the trypanosome cyanide-insensitive alternative oxidase. *Proc. Natl. Acad. Sci. USA*. In press
113. Shimizu H, Osanai A, Sakamoto K, Inaoka DK, Shiba T, et al. 2012. Crystal structure of mitochondrial quinol-fumarate reductase from the parasitic nematode *Ascaris suum*. *J. Biochem.* 151:589–92
114. Shinkarev VP. 2006. Ubiquinone (coenzyme Q₁₀) binding sites: low dielectric constant of the gate prevents the escape of the semiquinone. *FEBS Lett.* 580:2534–39
115. Siedow JN, Umbach AL, Moore AL. 1995. The active site of the cyanide-resistant oxidase from plant mitochondria contains a binuclear iron center. *FEBS Lett.* 362:10–14
116. Silverstein TP. 2011. Photosynthetic water oxidation versus mitochondrial oxygen reduction: distinct mechanistic parallels. *J. Bioenerg. Biomembr.* 43:437–46

117. Sluse FE, Jarmunzkiewicz W. 2004. Regulation of electron transport in the respiratory chain of plant mitochondria. In *Plant Mitochondria: From Genome to Function*, Adv. Photosynth. Respir. 17, ed. DA Day, AH Millar, J Whelan, pp. 231–46. Dordrecht: Springer
118. Sunderhaus S, Klodmann J, Lenz C, Braun H-P. 2010. Supramolecular structure of the OXPHOS system in highly thermogenic tissue of *Arum maculatum*. *Plant Physiol. Biochem.* 48:265–72
119. Szeto SSW, Reinke SN, Sykes BD, Lemire BD. 2007. Ubiquinone-binding site mutations in the *Saccharomyces cerevisiae* succinate dehydrogenase generate superoxide and lead to the accumulation of succinate. *J. Biol. Chem.* 282:27518–26
120. Umbach AL, González-Meler MA, Sweet CR, Siedow JN. 2002. Activation of the plant mitochondrial alternative oxidase: insights from site-directed mutagenesis. *Biochim. Biophys. Acta* 1554:118–28
121. Umbach AL, Siedow JN. 1993. Covalent and noncovalent dimers of the cyanide-resistant alternative oxidase protein in higher plant mitochondria and their relationship to enzyme activity. *Plant Physiol.* 103:845–54
122. Umbach AL, Siedow JN. 1996. The reaction of the soybean cotyledon mitochondrial cyanide-resistant oxidase with sulfhydryl reagents suggests that α -keto acid activation involves the formation of a thiohemiacetal. *J. Biol. Chem.* 271:25019–26
123. Umbach AL, Siedow JN. 2000. The cyanide-resistant alternative oxidase from the fungi *Pichia stipitis* and *Neurospora crassa* are monomeric and lack regulatory features of the plant enzyme. *Arch. Biochem. Biophys.* 378:234–45
124. Van Aken O, Giraud E, Clifton R, Whelan J. 2009. Alternative oxidase: a target and regulator of stress responses. *Physiol. Plant.* 137:354–61
125. van Dongren JT, Gupta KJ, Ramírez-Aguilar SJ, Araújo WL, Nunes-Nesi A, et al. 2011. Regulation of respiration in plants: a role for alternative metabolic pathways. *J. Plant Physiol.* 168:1434–43
126. Van Herk AWH. 1937. Chemical processes in *Sauromatum* flowers. *Proc. Acad. Sci. Amst.* 40:709–19
127. Van Herk AWH. 1937. Chemical processes in *Sauromatum* spikes. II. *Proc. Acad. Sci. Amst.* 40:607–14
128. Van Herk AWH, Badenhuisen NP. 1934. Respiration and catalase action in the *Sauromatum* spadix. *Proc. Acad. Sci. Amst.* 37:99–105
129. Vanlerberghe GC, McIntosh L. 1994. Mitochondrial electron transport regulation of nuclear gene expression. Studies with the alternative oxidase gene of tobacco. *Plant Physiol.* 105:867–74
130. Vanlerberghe GC, McIntosh L. 1996. Signals regulating the expression of the nuclear gene encoding alternative oxidase of plant mitochondria. *Plant Physiol.* 111:589–95
131. Vanlerberghe G, McIntosh L, Yip J. 1998. Molecular localization of a redox-modulated process regulating plant mitochondrial electron transport. *Plant Cell* 10:1551–60
132. Wendt KU, Poralla K, Schulz GE. 1997. Structure and function of a squalene cyclase. *Science* 277:1811–15
133. Wikström M. 2012. Active site intermediates in the reduction of O₂ by cytochrome oxidase, and their intermediates. *Biochim. Biophys. Acta* 1817:468–75
134. Wilkens S, Borchardt D, Weber J, Senior AE. 2005. Structural characterization of the interaction of the δ and α subunits of the *Escherichia coli* F₁F₀-ATP synthase by NMR spectroscopy. *Biochemistry* 44:11786–94
135. Wood PM, Hollomon DW. 2003. A critical evaluation of the role of alternative oxidase in the performance of strobilurins and related fungicides acting at the Q_o site of Complex III. *Pest Manag. Sci.* 59:499–511
136. Yabu Y, Yoshida A, Suzuki T, Nihei C, Kawai K, et al. 2003. The efficacy of ascofuranone in a consecutive treatment on *Trypanosoma brucei brucei* in mice. *Parasitol. Int.* 52:155–64
137. Yabu Y, Yoshida A, Suzuki T, Nihei C, Kawai K, et al. 2006. Chemotherapeutic efficacy of ascofuranone in *Trypanosoma vivax*-infected mice without glycerol. *Parasitol. Int.* 55:39–43
138. Yang XD, Yu L, He DY, Yu CA. 1998. The quinone-binding site in succinate-ubiquinone reductase from *Escherichia coli*: quinone-binding domain and amino acids involved in quinone binding. *J. Biol. Chem.* 273:31916–23

139. Yoshikawa S, Shinzawa-Itoh K, Nakashima R, Yaono R, Yamashita E, et al. 1998. Redox-coupled crystal structural changes in bovine heart cytochrome *c* oxidase. *Science* 280:1723–29
140. Zhang QS, Hoefnagel MHN, Wiskich JT. 1996. Alternative oxidase from *Arum* and soybean: its stabilization during purification. *Physiol. Plant.* 96:51–58
141. Zhang Z, Huang L, Schulmeister VM, Chi YI, Kim KK, et al. 1998. Electron transfer by domain movement in cytochrome *bc*₁. *Nature* 392:677–84
142. Zottini M, Formentin E, Scattolin M, Carimi F, Lo Schiavo F, et al. 2002. Nitric oxide affects plant mitochondrial functionality in vivo. *FEBS Lett.* 515:75–78



Contents

Benefits of an Inclusive US Education System <i>Elisabeth Gantt</i>	1
Plants, Diet, and Health <i>Cathie Martin, Yang Zhang, Chiara Tonelli, and Katia Petroni</i>	19
A Bountiful Harvest: Genomic Insights into Crop Domestication Phenotypes <i>Kenneth M. Olsen and Jonathan F. Wendel</i>	47
Progress Toward Understanding Heterosis in Crop Plants <i>Patrick S. Schnable and Nathan M. Springer</i>	71
Tapping the Promise of Genomics in Species with Complex, Nonmodel Genomes <i>Candice N. Hirsch and C. Robin Buell</i>	89
Understanding Reproductive Isolation Based on the Rice Model <i>Yidan Ouyang and Qifa Zhang</i>	111
Classification and Comparison of Small RNAs from Plants <i>Michael J. Axtell</i>	137
Plant Protein Interactomes <i>Pascal Braun, Sébastien Aubourg, Jelle Van Leene, Geert De Jaeger, and Claire Lurin</i>	161
Seed-Development Programs: A Systems Biology–Based Comparison Between Dicots and Monocots <i>Nese Sreenivasulu and Ulrich Wobus</i>	189
Fruit Development and Ripening <i>Graham B. Seymour, Lars Østergaard, Natalie H. Chapman, Sandra Knapp, and Cathie Martin</i>	219
Growth Mechanisms in Tip-Growing Plant Cells <i>Caleb M. Rounds and Magdalena Bezanilla</i>	243
Future Scenarios for Plant Phenotyping <i>Fabio Fiorani and Ulrich Schurr</i>	267

Microgenomics: Genome-Scale, Cell-Specific Monitoring of Multiple Gene Regulation Tiers <i>J. Bailey-Serres</i>	293
Plant Genome Engineering with Sequence-Specific Nucleases <i>Daniel F. Voytas</i>	327
Smaller, Faster, Brighter: Advances in Optical Imaging of Living Plant Cells <i>Sidney L. Shaw and David W. Ehrhardt</i>	351
Phytochrome Cytoplasmic Signaling <i>Jon Hughes</i>	377
Photoreceptor Signaling Networks in Plant Responses to Shade <i>Jorge J. Casal</i>	403
ROS-Mediated Lipid Peroxidation and RES-Activated Signaling <i>Edward E. Farmer and Martin J. Mueller</i>	429
Potassium Transport and Signaling in Higher Plants <i>Yi Wang and Wei-Hua Wu</i>	451
Endoplasmic Reticulum Stress Responses in Plants <i>Stephen H. Howell</i>	477
Membrane Microdomains, Rafts, and Detergent-Resistant Membranes in Plants and Fungi <i>Jan Malinsky, Miroslava Opekarová, Guido Grossmann, and Widmar Tanner</i>	501
The Endodermis <i>Niko Geldner</i>	531
Intracellular Signaling from Plastid to Nucleus <i>Wei Chi, Xuwu Sun, and Lixin Zhang</i>	559
The Number, Speed, and Impact of Plastid Endosymbioses in Eukaryotic Evolution <i>Patrick J. Keeling</i>	583
Photosystem II Assembly: From Cyanobacteria to Plants <i>Jörg Nickelsen and Birgit Rengstl</i>	609
Unraveling the Heater: New Insights into the Structure of the Alternative Oxidase <i>Anthony L. Moore, Tomoo Shiba, Luke Young, Shigeharu Harada, Kiyoshi Kita, and Kikukatsu Ito</i>	637
Network Analysis of the MVA and MEP Pathways for Isoprenoid Synthesis <i>Eva Vranová, Diana Coman, and Wilhelm Grussem</i>	665

Toward Cool C ₄ Crops <i>Stephen P. Long and Ashley K. Spence</i>	701
The Spatial Organization of Metabolism Within the Plant Cell <i>Lee J. Sweetlove and Alisdair R. Fernie</i>	723
Evolving Views of Pectin Biosynthesis <i>Melani A. Atmodjo, Zhangying Hao, and Debra Mohnen</i>	747
Transport and Metabolism in Legume-Rhizobia Symbioses <i>Michael Udvardi and Philip S. Poole</i>	781
Structure and Functions of the Bacterial Microbiota of Plants <i>Davide Bulgarelli, Klaus Schlaeppi, Stijn Spaepen, Emiel Ver Loren van Themaat, and Paul Schulze-Lefert</i>	807
Systemic Acquired Resistance: Turning Local Infection into Global Defense <i>Zheng Qing Fu and Xinnian Dong</i>	839

Indexes

Cumulative Index of Contributing Authors, Volumes 55–64	865
Cumulative Index of Article Titles, Volumes 55–64	871

Errata

An online log of corrections to *Annual Review of Plant Biology* articles may be found at <http://www.annualreviews.org/errata/arplant>